

Deep MMT¹Transit Survey of the Open Cluster M37 II: Variable Stars

J. D. Hartman², B. S. Gaudi³, M. J. Holman², B. A. McLeod², K. Z. Stanek³,
J. A. Barranco⁴, M. H. Pinsonneault³ and J. S. Kalirai^{5,6}

ABSTRACT

We have conducted a deep ($15 \gtrsim r \lesssim 23$), 20 night survey for transiting planets in the intermediate age (~ 500 Myr) open cluster M37 (NGC 2099) using the Megacam wide-field mosaic CCD camera on the 6.5m Multiple Mirror Telescope (MMT). In this paper we present a catalog and light curves for 1409 variable stars; 1395 (99%) of these are new discoveries. A substantial fraction ($\gtrsim 500$) of these variables are most likely rapidly rotating young low mass stars that are members of the cluster. We identify and analyze five particularly interesting individual variables including a previously identified variable which we suggest is probably a hybrid γ Doradus/ δ Scuti pulsator, an enigmatic white dwarf or subdwarf B star that shows pulsation like variations with a period of 0.157728 ± 0.00001 days and an amplitude of 0.07 mag in r , a possible quiescent cataclysmic variable, a detached eclipsing binary (DEB) with at least one γ Doradus pulsating component (only the second such variable found in an eclipsing binary), and a low mass ($M_P \sim M_S \sim 0.6M_\odot$) DEB that is a possible cluster member. A preliminary determination of the physical parameters for the DEB+ γ Doradus system yields $M_P = 1.58 \pm 0.04M_\odot$, $M_S = 1.58 \pm 0.04M_\odot$, $R_P = 1.39 \pm 0.07R_\odot$ and $R_S = 1.38 \pm 0.07R_\odot$.

²Harvard-Smithsonian Center for Astrophysics, 60 Garden St., Cambridge, MA 02138, USA; jhartman@cfa.harvard.edu, mholman@cfa.harvard.edu, bmcLeod@cfa.harvard.edu, jbarranc@cfa.harvard.edu

³Department of Astronomy, The Ohio State University, Columbus, OH 43210, USA; gaudi@astronomy.ohio-state.edu, kstanek@astronomy.ohio-state.edu, pinsono@astronomy.ohio-state.edu

⁴Department of Physics and Astronomy, San Francisco State University, 1600 Holloway Ave., San Francisco, CA 94132, USA; barranco@stars.sfsu.edu

⁵University of California Observatories/Lick Observatory, University of California at Santa Cruz, Santa Cruz CA, 95060

⁶Hubble Fellow

Subject headings: open clusters and associations:individual (M37) — surveys — stars:variables:other — binaries:eclipsing — stars:rotation — stars:fundamental parameters

1. Introduction

This paper is the second in a series of papers on a deep survey for transiting planets in the open cluster M37 (NGC 2099) using the MMT telescope. In the first paper (Hartman et al. 2007, Paper I) we introduced the survey, described the spectroscopic and photometric observations and the data reduction, determined the fundamental parameters (age, metallicity, distance and reddening) of the cluster, and obtained its mass and luminosity functions and radial density profile. As a result, we have a good understanding of the population of stars that we have observed. This paper focuses on the variable stars in our survey. We will discuss stellar rotation and transiting planets in future papers.

The study of variable stars in open clusters is particularly interesting since one can put constraints on the age, metallicity, distance and reddening of stars that are cluster members. This additional information allows for powerful tests of stellar pulsation models (e.g. Frandsen and Arentoft 1998), or stellar evolution theory in the case of eclipsing binaries (e.g. Southworth, Maxted, & Smalley 2004). By identifying variables in different clusters it is possible to study the evolution of stellar properties including rotation (e.g. Irwin et al. 2006, 2007) and pulsation (e.g. Krisciunas 1998). Even if most stars in a given survey are not members of a cluster, identifying the variables is still interesting as it is a good tool for finding rare or previously unknown phenomena that deserve detailed study.

M37 has been the target of two previous surveys for variable stars (Kiss et al. 2001; Kang et al. 2007) which have discovered 24 variables. In part because our survey goes substantially deeper than either of these, we have identified 1409 variables, of which 1395 are new discoveries.

In the following section we will briefly describe the data and in §3 we describe the selection of variable stars and present the catalog. In §4 we match to the previously identified variables. In §5 we discuss the global properties of the variables noting that a substantial

¹Observations reported here were obtained at the MMT Observatory, a joint facility of the Smithsonian Institution and the University of Arizona.

fraction of these stars are likely to be rapidly rotating spotted stars that are members of the cluster. In §6 we analyze five particularly interesting variables including a probable hybrid γ Doradus/ δ Scuti pulsator, an enigmatic white dwarf or subdwarf B star that shows pulsation like variations with a period > 0.1 days and an amplitude of ~ 0.1 mag, a possible quiescent cataclysmic variable, a detached eclipsing binary with a γ Doradus component and a low mass detached eclipsing binary with $\sim 0.6M_{\odot}$ components that is a possible cluster member. Finally we summarize our results in §7.

2. Summary of Observations

A detailed discussion of the observations and data reduction for our survey were presented in Paper I, we provide only a brief overview here. The observations consist of both *gri* photometry for ~ 16000 stars, and *r* time-series photometry for ~ 23000 stars obtained with the Megacam mosaic imager (McLeod et al. 2000) on the 6.5 m MMT and high-resolution spectroscopy of 167 stars obtained with the Hectochelle multi-fiber, high-dispersion spectrograph (Szentgyorgyi et al. 1998) on the MMT.

The primary time-series photometric observations were done using the *r* filter and consist of ~ 4000 high quality images obtained over twenty four nights (including eight half nights) between December 21, 2005 and January 21, 2006. We obtained light curves for stars with $14.5 \lesssim r \lesssim 23$ using a reduction pipeline based on the image subtraction technique and software due to Alard and Lupton (1998) and Alard (2000). We apply two cleaning routines to the data: clipping bad points and removing individual bad images. We do not decorrelate against other systematic variations since doing so tends to distort the light curves of large amplitude variables.

Where available we took *BV* photometry for the sources from Kalirai et al. (2001). We also transformed our *ri* photometry into I_C using the I_C photometry from Nilakshi and Sagar (2002) to define the transformation. Finally we took K_S photometry from 2MASS (Skrutskie et al. 2006) where available.

The spectra were obtained on four separate nights between February 23, 2007 and March 12, 2007 and were used to measure T_{eff} , $[Fe/H]$, $v \sin i$ and the radial velocity (RV) via cross-correlation.

3. Variable Star Selection

We have used the following three different methods to identify periodic variable stars from our time series observations:

1. A search for periodic, sinusoidal variations with the Lomb-Scargle (L-S) algorithm (Lomb 1976; Scargle 1982; Press and Rybicki 1989; Press et al. 1992).
2. A search for general periodic variability using the analysis of variance (AoV) periodogram due to Schwarzenberg-Czerny (1996), as implemented by Devor (2005).
3. A search for eclipses using the Box-fitting Least Squares (BLS) algorithm due to Kovács, Zucker and Mazeh (2002).

While there will be overlap between the results of these methods, each algorithm tends to be sensitive to different types of variables. The more general tool, AoV, should in principle identify variables found by the more restrictive L-S and BLS algorithms, but it may also be more sensitive to non-astrophysical variability due to uncalibrated instrumental or atmospheric effects. As a result, AoV cannot be used to search for variability with amplitudes as low as that accessible to L-S and BLS. In the next three subsections we describe the results from using each selection tool, and in the last subsection we present the composite catalog of variables.

3.1. L-S search

We used the L-S algorithm to search for sinusoidal periodic variables with periods between 0.01 and 20 days; the search was conducted with a sampling of 0.005 times the Nyquist sampling. Figure 1 shows the histogram of peak frequencies for all of our light curves. Spikes in the histogram result from instrumental or atmospheric artifacts that systematically affect numerous light curves. Many of these occur at aliases of 1 sidereal day and result from artifacts such as the rotation of diffraction spikes from nearby stars or color dependent extinction. Other artifacts, such as a series of observations where the image subtraction procedure did not work optimally (due, for example, to coma or other non-symmetric distortions of the PSF) may be phased at periods that are not aliases of a sidereal day. Since the vast majority of candidate variables identified at these frequencies are spurious detections, we reject any detection at one of these spikes. The rejection removes 8225 of the 23790 light curves. The lower panel of figure 1 shows the histogram after removing these frequencies. The rise in the number of detections towards short frequencies results both from real variables with periods

between 5 and 10 days and from $\sim 1/f$ red noise (e.g. Pont, Zucker and Queloz 2006) in the light curves.

For each light curve we calculate the false alarm probability (FAP) of the period corresponding to the peak in the periodogram using equation 13.8.7 from Press et al. (1992). For convenience we refer to $\log(FAP)$ as FAP. The FAP provides a relative ordering of detection confidence among the light curves. How the formal FAP relates to the real FAP depends on the specific window function of the observations as well as on the noise distribution in the light curves. As the noise in our light curves is typically not frequency independent we do not expect the formal FAP to correspond to the real FAP, thus the selection threshold in formal FAP is set by inspecting the light curves at a range of FAP values.

In figure 2 we plot the histogram of formal FAP values together with example light curves at a range of values. Only stars detected in all three filters (*gri*), with more than 500 points in their light curves, and with $r < 20$ are included in the histogram. We adopt a selection criterion of $FAP < -150$ for reliable detections. This selects 1516 candidate variables.

Note that while the formal false alarm probability for these detections is an astonishingly small 10^{-150} , the actual false alarm probability is much higher due to red noise. While methods such as the trend filtering algorithm (TFA; Kovács, Bakos and Noyes 2005) or Sysrem (Tamuz, Mazeh and Zucker 2005) may filter red noise from an ensemble of light curves, they are known to distort the signal of large amplitude variables and may reduce the sensitivity to these variables as well. Since we are primarily interested in large amplitude variables, we do not apply either of these filtering methods to our light curves. A filtering method will be applied to the light curves before searching for planetary transits and other low amplitude variables; the results from this will be presented in a separate paper.

3.2. AoV search

We used the AoV algorithm to search for variables with periods between 0.1 and 20 days; a coarse scan was conducted at 0.01 times the Nyquist sampling with a fine tuning search around the highest peaks at 0.0005 times the Nyquist sampling. Following the Devor (2005) implementation, we normalize the AoV periodogram of each light curve to have zero mean and unit variance. As for L-S, we first reject spikes in the frequency histogram (removing 8968 light curves, figure 3) and set the selection criterion by visual inspection of light curves. Figure 4 shows the histogram of normalized AoV values together with example light curves. We adopt a selection criterion of $AoV > 3.75$ which selects 982 candidate variables.

3.3. BLS search

We search for eclipsing variables using the BLS algorithm. The search is restricted to periods between 0.2 and 5.0 days as the detection efficiency drops for longer periods. As for L-S and AoV we first reject bad periods by searching for spikes in the histogram of detected periods (5621 light curves are rejected; see figure 5).

Following Pont, Zucker and Queloz (2006) we use as our selection statistic the signal to pink noise:

$$SN^2 = \frac{\delta^2}{\sigma_w^2/n_t + \sigma_r^2/N_t} \quad (1)$$

where δ is the depth of the eclipse, n_t is the number of points in the eclipse, N_t is the number of distinct eclipses sampled, σ_w is the white noise, and σ_r is the red noise at the time-scale of the eclipse. We subtract the best BLS model from each light curve and set σ_w equal to the standard deviation of the residual. We then bin the residual light curve in time with a binsize equal to the duration of the eclipse and set σ_r equal to its standard deviation.

Figure 6 shows a histogram of the resulting SN values for all light curves, together with sample light curves at a range of SN values. We select 90 light curves with $SN > 12.0$ as candidate variables.

3.4. Estimation of the Period Errors

For the variables with periods detected by L-S or AoV, we measured the period uncertainty by bootstrap. For each bootstrap iteration we draw a sample of points from the light curve with replacement and then search for the period within a frequency of $\pm 1/T$ from the period found for the original light curve, where T is the time-baseline of the light curve. The period uncertainty for a light curve is given by the standard deviation of 100 bootstrap iterations. Figure 7 shows the period uncertainty of the variables as a function of their period.

We can estimate the expected uncertainty on the period using equation 25 of Schwarzenberg-Czerny (1991):

$$\Delta P \sim P^2 \sqrt{\frac{3\sigma^2 D}{T^3}} \quad (2)$$

where P is the period, σ is the noise in units of the signal amplitude (i.e., the inverse of the signal to noise), D is the average correlation time-scale for the residuals from the model periodic signal (equal to the sampling time for the case of pure gaussian white noise with a perfect sinusoidal signal), and T is the time base-line. This relation holds for $T \gg P \gg D$.

Note that the period error does not include uncertainties due to aliasing - it describes how well you can centroid the peak in a periodogram after choosing amongst aliases. We choose by eye the best period for each light curve from among the possible aliases.

We plot equation 2 on figure 7 for $T = 31.1$ days, assuming a typical signal to noise of 10 and a correlation time-scale of half an hour. Note that D is effectively a free parameter, since it is difficult to know a priori how well the AoV “model” will fit the actual light curves, and it is adjusted to provide a good fit to the short period errors. The errors from the bootstrap appear to be in reasonable agreement with theoretical expectations, though only if we allow for time-correlated noise. The disagreement for the longer period detections is due to the violation of the assumption $T \gg P$.

3.5. Combined Catalog of Variables

The combined list of candidate variables contains 1946 sources. Of these, 38 were detected by all three methods, 544 were detected by AoV and L-S but not by BLS, 6 were detected by L-S and BLS but not by AoV, 16 were detected by AoV and BLS but not by L-S, 384 were detected only by AoV, 928 were detected only by L-S, and 30 were detected only by BLS.

Before proceeding we must first correct for the blending of variability between sources that results from performing aperture photometry on the subtracted images (e.g. Hartman et al. 2004). To do this we identify groups of candidate variables that lie within $4''$ of each other (so that their PSFs may overlap significantly). We then choose from each group the source with the smallest average deviation of the centroid position measured on the subtracted images from the star’s position measured on the reference image. After this procedure we are left with 1811 candidate variables. Requiring that the variables be detected in the g , r and i filters reduces this number to 1692.

We then examine all candidate light curves by eye, choosing among the possible periods the one that appears to phase the light curve most cleanly, and rejecting false positive detections. After this procedure we are left with 1409 variables, of which 1347 have periods (note that variables without periods correspond to light curves which showed believable variability but for which the period returned by the selection tools did not appear to be correct). In figure 8 we show examples of some of the 283 light curves which were rejected by eye. Note that some of these may well be real variables, and unfortunately the selection process is fairly subjective, however it is very difficult to develop an automatic selection routine that is robust against false positives when dealing with real data.

Table 1 gives the first few entries in our catalog of variable stars, the full catalog is available in the electronic edition of the journal. We continue the numbering system from Kiss et al. (2001), relabeling KV1 through KV17 from Kang et al. (2007) as V8-V24 and labeling new variables beginning with V25. The new variables are sorted by RA. For completeness we include unmatched known variables, though we caution that the coordinates for V8-10, V15-16, V18, and V23 are uncertain since we did not observe these stars and there appears to be an error in the table listing the variable star coordinates in Kang et al. (2007) (see next subsection). Light curves for all variable stars are available on request. Table 2 provides a summary of the variable star catalog.

4. Match to Known Variables

There are a total of twenty four variables that have been previously identified in the field of M37. Of these, seven were found by Kiss et al. (2001) and an additional seventeen were found by Kang et al. (2007). Thirteen of these variables are eclipsing binaries, ten show δ -Scuti type variations and one is an RRc variable.

We obtained light curves for fifteen of the known variables. Six of the unmatched variables (V1-2, V8-10 and V18) are saturated in our observations, the other three unmatched sources (V15-16, and V23) fell on chip gaps and were not observed. Of the fifteen matched variables, we independently select fourteen of them as variables. In matching to the known variables we found that there appears to be a discrepancy between the coordinates for several of the KV variables listed in table 1 of Kang et al. (2007) and the light curves presented in that paper. We revise the coordinates in our own catalog following the naming convention used for the light curves in Kang et al. (2007).

The one variable that we observed but did not recover is V12. For this source the peak signal detected by L-S is at a period of 0.07857908 days with an FAP of -96.2, which does not pass our selection threshold. This is at the same period found by Kang et al. (2007), however the amplitude is 9 mmag in our r light curve compared to 15 mmag in the Kang et al. (2007) V light curve. Nonetheless the signal is easily detected in our light curve. The selection criterion of $FAP < -150$ is quite conservative for periods less than 1 day and it is possible that a number of additional short period variables could be identified by adopting a period dependent selection threshold.

Figure 9 shows our light curves for the fourteen variables that we recover together with the published photometry from Kiss et al. (2001). For the variables V3-V7 we combine our photometry with the Kiss et al. (2001) photometry which was taken between Dec. 1999,

and Feb. 2000 to improve the precision of the periods. We will now discuss a few of these variables in detail, though we leave the very interesting star V17 for §6.

4.1. V3 and V4

The contact eclipsing binaries V3 and V4 both exhibit a pronounced O’Connell effect (unequal maxima; O’Connell 1951). The origin of this effect is still uncertain, though a number of theories have been put forward to explain it including stellar spot activity (Binnendijk 1960), the formation of a hot spot on one of the stars due to mass exchange (Shaw 1994), or an unequal interaction between the two components and any circumstellar material (Liu and Yang 2003). In any of these theories, one would expect the effect to be variable. V4 does show some evidence for variation of ~ 0.01 mag between the 2000 and 2006 epochs as well as within the 2006 epoch as seen in figure 10; V3 on the other hand, does not show evidence of variation.

4.2. V19

Kang et al. (2007) classify this variable as a possible W UMa type eclipsing binary, though the classification is unsecure due to a lack of phase coverage. We find that the light curve shows substantial amplitude variations which make it most likely a fundamental mode RR Lyrae pulsator with the Blazhko effect.

5. Properties of the Variables

In figure 11 we show the location of the variables on gr and gi CMDs. It is immediately apparent that the variables lie preferentially along the cluster main sequence. Most of these are rapidly rotating stars (relative to the Sun) with surface brightness inhomogeneities that are detectable at our level of photometric precision. We discuss these variables in detail in a companion paper (Hartman et al. 2007, in preparation). Given the relatively young age of the cluster (500 Myr), the fact that we detect these variations for so many cluster stars is not surprising.

From inspecting the light curves, we classify 24 of the variables as eclipsing binaries (or ellipsoidal variables) and 21 of the variables as pulsating variables with periods less than 1 day. Including the 4 previously identified eclipsing binaries and 6 previously identified pulsating stars that we have not observed, there are total of 28 eclipsing binaries and 27

pulsating stars known in the field of this cluster. We show the locations of these variables on the gr and gi CMDs in figure 12 and show the phased light curves for the newly discovered variables in figures 13 and 14. As the red-edge of the δ -Scuti instability strip intersects the M37 main sequence at $V \sim 14.4$ or $r \sim 14.2$ (Kang et al. 2007), we expect that any δ -Scuti variables within this cluster will be saturated in our time series observations. The one or two pulsating variables in figure 12 that lie near the cluster main sequence are thus likely to be background disk stars. There are six eclipsing binaries that lie near the cluster main sequence, these include V3, V4, V675, V834, V1002 and V1345. The binaries V3, V4 and V834 are contact systems, while V675, V1002 and V1345 are detached systems. We will discuss V1002 and V1345 in greater detail in §6.4 and 6.5.

We have obtained spectra for the system V675 and detected it as a single lined spectroscopic binary. The cross-correlation routine gives a temperature for this system of ~ 7000 K which is too hot for it to be a member of the cluster given its position on the CMD, but consistent with it being a member of the background field. Based on the radial velocity curve, we estimate that the systemic RV is ~ -2 km/s compared with 9.2 ± 1.4 km/s for the cluster (Paper I). We conclude that this system is not a member of the cluster, and will not investigate it any further.

Figure 15 shows the period- r relation for the variables. In two of the panels we split the variables into two groups, those which match to photometrically selected cluster members (see Paper I), and those which lie well away from the cluster main sequence. There is a strong correlation between period and magnitude for the cluster members with a break into two groups at $r \sim 18$. We are most likely seeing the relation between rotation period and stellar mass for the young cluster stars. The relation is quite similar to that seen, for example, in the Hyades by Radick et al. (1987), and will be discussed in greater detail elsewhere. The non-cluster members appear to show no clear correlation between period and magnitude. This is not unexpected, though, since the field stars lie over a large range of distances from the Earth.

We will now discuss a few of the populations of field variables.

5.1. Short Period Pulsators

The majority of the short-period pulsating variables appear to lie in the range $r < 19$, $0.2 < g - r < 1$. These stars have pulsation periods on the order of 0.1 days and have $0.45 < B - V < 1.18$, they are thus likely to be background δ -Scuti or SX Phe (Population II δ -Scuti) stars largely seen through $E(B - V) > 0.4$.

Fundamental mode δ -Scuti variables exhibit a well-known period-luminosity-color (PLC) relation that we can use to determine their distances. McNamara et al. (2000) give the following period-color and period-luminosity relations:

$$(V - I_C)_0 = 0.195 \log P + 0.514, \quad (3)$$

$$M_V = -3.725 \log P - 1.933. \quad (4)$$

The first of these equations can be used to determine the $E(V - I_C)$ reddening, then assuming $E(V - I_C) = 1.55E(B - V)$ (Paper I) and $A_V = 3.1E(B - V)$ we can determine the distance using equation 4.

We identify four stars, based on their periods, amplitudes and light curve shapes, that are quite likely fundamental mode pulsators. We give the identifications, colors, periods and inferred distances in table 3, the BV photometry for V6 comes from Kang et al. (2007) as this star was not observed by Kalirai et al. (2001). We include V5 in this list, though we note that Kang et al. (2007) have argued that this star may be an RRc variable rather than a fundamental mode δ -Scuti. Figure 16 shows the distance and extinction for these four stars as well as for a number of eclipsing binaries discussed below. One star lies well beyond the disk of the galaxy and is likely to be a halo SX Phe star. The total extinction in this direction appears to be $A_V \sim 2$ mag, or $E(B - V) = 0.65$ which is slightly larger than the value of $E(B - V) = 0.56$ from the Schlegel, Finkbeiner and Davis (1998) extinction maps (note that the galactic latitude of the field is $\sim 3^\circ$, so the Schlegel, Finkbeiner and Davis (1998) map is unreliable here).

5.2. Eclipsing Binaries

As seen in figure 14, many of the eclipsing binaries are contact, W UMa type systems. Similar to δ -Scuti variables, these binaries exhibit a PLC relation that we can use to determine their distances. We adopt the following PLC relation from Rucinski and Duerbeck (1997):

$$M_V = -2.38 \log P + 4.26(B - V)_0 + 0.28 \quad (5)$$

where we assume solar metallicity, and note that the resulting uncertainty on the distance modulus for each source is ~ 0.5 mag.

The reddening of each system can be estimated from the $B - V - V - I_C$ color-color plot assuming $E(V - I_C) = 1.55E(B - V)$ and using the fiducial relation for the cluster. Assuming $A_V = 3.1E(B - V)$, we can then find the distance to the system from equation 5. Table 4 gives the identifications, colors, periods and inferred distances and extinctions for

10 candidate contact binary systems. We do not include two systems which appear to have unreliable photometry (one has a negative reddening, the other yields $A_V > 4.0$ mag), and one star which has dereddened colors that are blueward of the cluster turnoff.

Figure 16 shows A_V as a function of distance for the 10 systems listed in table 4. The W UMa systems appear to show more scatter than the δ -Scuti stars which may be attributed in part to the 0.5 mag uncertainty in the $P - L$ relation for these stars and in part to the greater uncertainty in their colors due to their larger amplitude variability. There is also a hint that the W UMa systems have systematically greater extinction at a given distance than what we infer from the δ -Scuti stars. It is unclear what the source of this systematic discrepancy might be.

We also show the extinction vs. distance from the Besançon model (Robin et al. 2003) for the galactic latitude/longitude of the field ($l = 177.6^\circ$, $b = 3.1^\circ$), assuming the default interstellar extinction of 0.7 mag/kpc. While the value of 0.7 mag/kpc appears to reproduce the extinction of the cluster, the model extinction/distance relation cuts off sharply at the scale-height of the galactic disc (~ 140 pc) whereas the observed relation cuts off at about twice that distance. The model assumes that the dust follows a simple exponential density profile in both the radial and vertical directions; discrete clouds along the line of sight with higher than average density may cause the total extinction in this field to be greater than expected.

5.3. Rotating Field Stars

There are ~ 500 variable stars that do not appear to be members of the cluster, are not eclipsing binaries, and are not δ -Scuti or RR Lyrae type pulsators. We argue that most of these stars are likely to be rotating variable main sequence stars.

In figure 17 we plot period against $V - I_C$ for the 479 of these variables that have period determinations and V photometry. For stars with $1 < V - I_C < 2.3$ the periods appear to scatter between 0.1 and 20 days, with the highest density between 3 and 12 days, while stars with $V - I_C < 1$ or $V - I_C > 2.3$ tend to have shorter periods (< 2 days for stars with $V - I_C > 2.3$). The trend toward shorter periods among the bluer stars may either indicate a population of pulsators (e.g. γ Doradus stars) or it may indicate shorter rotation periods for the hotter stars. From a visual inspection of the light curves alone it is impossible to distinguish between these two cases. For the redder stars, however, the trend toward shorter periods is probably due to the onset of short period rotation for cool stars. Note that for the cluster, $V - I_C = 2.3$ corresponds roughly to $r \sim 20$, which, as seen in the center

panel of figure 15, is where the stars appear to transition to a population of predominately short period rotators. The scatter between 3 and 12 days is also consistent with the range of rotation periods seen for brighter stars, keeping in mind that as the rotation periods increase the amplitudes decrease (thus making longer period rotators harder to detect) and that the rotation periods generally evolve over time from rapid rotation in the pre-main sequence stage to month long rotations for stars the age of the sun (e.g. Irwin et al. 2007).

One way to test the consistency of our hypothesis that these variables are rapidly rotating, heavily spotted stars is to compare the amplitudes of their light curves to the Rossby number (R_o ; the ratio of the rotation period to the convective turnover time-scale). Empirically there is a strong anti-correlation between the Rossby number and the x-ray activity of low-mass stars (Noyes et al. 1984), and a similar anti-correlation appears to hold for the light curve amplitudes of spotted rotating stars as well (e.g. Messina, Rodonò and Guinan 2001).

The turnover time-scale can be estimated from the empirical relation given by Noyes et al. (1984). To apply this relation we must first de-redden our stars. As for the W UMa stars, this can be done using the $B - V$ vs. $V - I_C$ color-color plot together with the fiducial de-reddened relation for the cluster (figure 18). Because the reddening vector for stars with $B - V > 1.2$ or $V - I_C > 1.8$ may intersect the fiducial curve at more than one location, we select stars bluer than these limits. We also adopt a cut on the inferred $E(B - V)$ of $0 < E(B - V) < 0.7$ and a magnitude cut of $15 < V < 22$. To avoid including stars without surface convection zones we also only consider stars with $(B - V)_0 > 0.5$. This last cut rejects 25 stars, many of which may be γ Doradus variables.

In figure 19 we show the relation between R_o and the peak-to-peak r -band amplitude (A_r) for the 221 stars which pass the above cuts (we also reject one star with $R_o \sim 2$ as it is an outlier from the rest of the observed stars). By eye there is a clear anti-correlation. To show that this is not due to a selection effect, we also plot for each star the estimated minimum amplitude that the light curve could have had and still have passed the variable star selection criteria. The methods for calculating the amplitude of the light curves and estimating the minimum detectable amplitudes will be described elsewhere (Paper III). To evaluate the significance of the apparent correlation we calculate Kendall's normalized rank-based τ correlation coefficient, modified for the case of data suffering a one-sided truncation (Tsai 1990; Efron and Petrosian 1992, 1999). We find $\tau = -2322$ meaning the null hypothesis of no correlation is formally rejected at the 2322σ level. This correlation is stronger than what we find for the period- A_r ($\tau = -1728$) or for the $(B - V)_0$ - A_r ($\tau = 550$) correlations. The anti-correlation between R_o and A_r is consistent with the hypothesis that rotation coupled with surface brightness inhomogeneities is the cause of the observed brightness variations for

these stars.

6. Individual Variable Stars

So far we have focused primarily on groups of variables. In this subsection we will investigate a few particularly interesting individual variables, including a very blue pulsating star with $g - r < 0.$, a blue flaring variable, and two detached eclipsing binaries that potentially are cluster members.

6.1. V17

Kang et al. (2007) emphasize the curious nature of the variable V17. They find two independent frequencies in its light curve: one at $f_1 = 22.796 \text{ day}^{-1}$ with a semi-amplitude of 32.9 mmag in V , and a second much lower frequency of $f_2 = 2.396 \text{ day}^{-1}$ with a semi-amplitude of 24.2 mmag in V . Kang et al. (2007) give two possible interpretations for this variable, that it is a hybrid γ Doradus/ δ Scuti type pulsator, or that it is a close semi-detached binary system with a δ Scuti primary and a late-type giant secondary showing ellipsoidal variations. They claim that the 2MASS color for the object suggests a late G or early K spectral type leading them to conclude that the binary hypothesis is more likely.

To aid in understanding this interesting object we have conducted a multi-frequency analysis of our r light curve using the Discrete Fourier Transform (DFT) with the CLEAN deconvolution algorithm (Roberts, Lehár and Dreher 1987). Figure 20 shows the DFT power spectrum before and after implementing CLEAN; we also show the power spectrum of the window function for reference. We confirm the high-frequency signal at $f_1 = 22.796 \text{ day}^{-1}$ and we find four additional low frequencies of $f_2 = 1.418 \text{ day}^{-1}$, $f_3 = 2.263 \text{ day}^{-1}$, $f_4 = 2.054 \text{ day}^{-1}$, and $f_5 = 0.823 \text{ day}^{-1}$. None of these frequencies are harmonics of each other. The error on all of these measurements is $\sim 0.003 \text{ day}^{-1}$.

After identifying the frequencies using DFT/CLEAN we fit a series of cosinusoids to the light curve of the form:

$$r = r_0 + \sum_{i=1}^7 a_i \cos(2\pi f_i(t - t_0) + \Phi_i) \quad (6)$$

to get the semi-amplitude and phase of each mode. For consistency with Kang et al. (2007) we adopt $t_0 = 2453000.0$. We find semi-amplitudes of $a_1 = 26.4 \text{ mmag}$, $a_2 = 13.7 \text{ mmag}$, $a_3 = 12.8 \text{ mmag}$, $a_4 = 12.9 \text{ mmag}$, and $a_5 = 11.2 \text{ mmag}$, and phases $\Phi_1 = 2.854$, $\Phi_2 = 1.132$,

$\Phi_3 = 4.866$, $\Phi_4 = 4.757$, $\Phi_5 = 5.477$. Alternatively, if we assume only the two frequencies from Kang et al. (2007) of $f_1 = 22.796 \text{ day}^{-1}$ and $f_2 = 2.396 \text{ day}^{-1}$ we find $a_1 = 27.2 \text{ mmag}$, $a_2 = 8.0 \text{ mmag}$, $\Phi_1 = 2.144$, and $\Phi_2 = 1.996$.

The presence of multiple frequencies in the range $0.8 < f < 2.3$ indicates that the low frequency variations are not due to ellipsoidal variability, and is instead suggestive of γ Doradus pulsations. This is not in conflict with the color of the star since the late-G/early-K spectral type estimate by Kang et al. (2007) assumes no reddening. Taking $B - V = 0.6$ from Kalirai et al. (2001) and noting that the reddening to the source must be at least the cluster value of $E(B - V) > 0.21$ given that the star lies below the cluster main sequence on the CMD, we find $(B - V)_0 < 0.39$ which, for a dwarf star, corresponds to a spectral type earlier than F5 (e.g. Schmidt-Kaler 1982). We conclude therefore that the star may very well be a hybrid γ Doradus/ δ Scuti pulsator. These stars are particularly interesting for astroseismology and to date only a handful of them are known (see King et al. 2006).

6.2. The Enigmatic Hot Variable V1119

As seen from its position on the CMD, star V1119 is an outlier with respect to the general population of variables found in our survey (figure 12). The star has $g - r = -0.396 \pm 0.013$, $r - i = -0.247 \pm 0.015$, $r = 19.97 \pm 0.012$, $B - V = -0.071 \pm 0.004$ and $V = 19.770 \pm 0.003$. This places the star roughly 2 magnitudes above the cluster white dwarfs. As seen in figure 13 the star shows saw-tooth like variability with a period of 0.157728 ± 0.000010 days and an amplitude of 0.07 mag in r .

While the position of the star on the CMD is consistent with it being a foreground white dwarf, the period is nearly an order of magnitude longer than the longest seen for white dwarf pulsations (the longest periods being 5-50 minutes for GW Vir stars which are still embedded in planetary nebulae, see Córscico, Althaus and Miller Bertolami 2006). Such a long period could be possible for a binary system, with the variations resulting from the reflection and/or ellipticity effects. However, the sawtooth appearance of the light curve suggests that the variations are due to pulsation.

Since the star cannot have $(B - V)_0 < -0.33$ (Schmidt-Kaler 1982), the maximum reddening that it could be seen through is $E(B - V) = 0.26$ ($A_V = 0.8$). From figure 16, we can estimate that the star must be closer than ~ 5 kpc assuming that the star lies along an average line of sight. We can therefore put a limit on its absolute magnitude of $M_V \gtrsim 5.5$. This rules out a main sequence star which must have $M_V \lesssim 1.1$ given the color (Schmidt-Kaler 1982). Even if there were no extinction, if the star were on the main

sequence it would have to be at least ~ 50 kpc away, placing it well beyond the disk of the galaxy, or ~ 300 kpc assuming at least the reddening of the cluster. It is possible that the object could be a hypervelocity B star which has been ejected from the galaxy, these have been found at distances of 50-100 kpc (e.g. Brown et al. 2007); though if this is the case the extinction to the star would have to be anomalously low. It is interesting to note, though, that the light curve shape, period, amplitude and color are all consistent with the star being a main sequence β -Cephei variable (Sterken and Jerzykiewicz 1993).

It is possible that the source is a sub-dwarf B (sdB) star, though the typical absolute magnitude of an sdB is $M_V \sim 4.6$ or brighter (Moehler, Heber and Rupprecht 1997) which is slightly brighter than the limit we set based on the maximum extinction for the source. There is a class of pulsating sdB stars, called PG 1716 stars, with periods comparable to what we see for V1119 (Green et al. 2003). These stars pulsate in high-order g-modes and typically have very low amplitudes (1 mmag or less), with the highest observed amplitudes of ~ 4 mmag (Kilkenny et al. 2006). If V1119 is a member of this class, then its amplitude is more than an order of magnitude larger than the other members its class. Such a large amplitude would be unusual for a high order g-mode pulsator since it would have to be pulsating in a very low degree l mode.

Perhaps a more likely explanation is that the star is a blend between a white dwarf or an sdB star and a much fainter variable. If the variable is a background δ -Scuti or SX Phe star, the period and light curve shape suggest that it would be a fundamental mode pulsator. In that case we can estimate its intrinsic color and magnitude using equations 3 and 4. This yields $(V - I_C)_0 = 0.36$, and $M_V = 1.05$, or $B - V \sim 0.3$. Assuming a minimum apparent $B - V$ of -0.33 for the white dwarf/sdB star, and an extinction of $A_V = 2.0$ mag to the δ -Scuti, the δ -Scuti must have $V \gtrsim 21$, and be $d \gtrsim 40$ kpc away. As seen in figure 16 there does appear to be an unblended SX Phe star at $d \sim 33$ kpc, and it is possible that there could be an even more distant one that happens to lie along the line of sight to a white dwarf.

The chances for a random blend of this nature though are rather low. Out of the 16431 point sources detected in our field with g , r and i measurements and with $r < 24$, there are 128 pairs of objects that are separated by $0.1 - 1''$. We do not detect any evidence that the object is anything other than a point source, so if the objects are within two magnitudes of each other then we estimate that they must be separated by $0''.1$ at the most. We would expect ~ 1 such random pairing out of all point sources in our field. The chances that one of the paired objects is a white dwarf and the other is a distant halo SX Phe star (both fairly rare in our field) is thus very low.

Alternatively, the variable star may be a short period rotating K or M dwarf (§5.3) that

is in a binary system with a white dwarf or sdB star. Such a pairing is more likely than the chance alignment of a white dwarf with a distant halo SX Phe star. A period of 0.157 days would be on the short side for such a star (see figure 17), though double this period would also be permissible since the star may have multiple spots. The shape of the light curve is similar to that seen for other variables in the cluster. The spotted cluster stars have amplitudes $A_r < 0.2$ mag; taking this as the maximum amplitude for a spotted star in the r -band we put an upper limit on the difference in magnitude between the companion and the white dwarf of $r_{comp} - r_{WD} < 0.6$ mag. The minimum $g - r$ value that a star can have is $g - r = -0.6$ (see Girardi et al. 2004), so to reproduce the color of the system the companion would have to have $g - r < 0.09$ (i.e. F0 or earlier). Therefore, this hypothesis appears to be inconsistent with the observations.

Understanding the nature of this variable will require spectroscopy to determine $\log(g)$ and T_{eff} of the hot star and to check for evidence of a blend with a cooler star.

6.3. V876

The light curve of the variable V876 is quite unique relative to the other variables in the survey. The light curve shows continuous non-periodic variability with a number of relatively small amplitude outbursts (0.1 – 0.2 mag). The typical duration of these outbursts is 0.5 days with a time-scale between outbursts of 1-2 days. The variation seen in this source is similar to the flickering seen in many cataclysmic variables (see Duerbeck 1996), confirming this identification would require additional observations including spectroscopy. The source matches to 2mass05523126+3236324 and has $B - V = 0.604$, $V = 16.090$, $g - r = 0.474$, $r - i = 0.208$, $r = 15.876$, $J - K_S = 0.311$, $H - K_S = 0.110$ and $K_S = 14.374$. We estimate that the reddening to the object is $E(B - V) \sim 0.29$.

6.4. Detached Eclipsing Binary V1345

The eclipsing binary V1345 is one of two detached eclipsing binaries that lie near the cluster main sequence. V1345 matches to 2mass05531108+3224434, it has an orbital period of 2.1916 ± 0.0016 days, and photometry $B - V = 0.594$, $V = 14.952$, $g - r = 0.42$, $r - i = 0.15$, $r = 14.79$, $J - K_S = 0.331$, $H - K_S = 0.084$, and $K_S = 13.331$. The source is just at our saturation threshold, and in many of the images it is saturated, so there are only 1111 points in its light curve (a factor of ~ 4 fewer than most light curves). If the system is a member of the cluster, its primary star would have $M \sim 1.2M_\odot$ based on its r magnitude

and assuming equal mass components. We note, however, that the star does appear to be slightly below the main sequence, so its photometric membership is questionable.

To determine the period of the out of eclipse variations, we remove the in-eclipse points from the light curve and, using L-S, find a period of 0.939 ± 0.01 days with a peak-to-peak amplitude of 0.019 mag. We subtract a sinusoid fit to this signal and find in the residual light curve an additional period of 1.166 ± 0.01 days with an amplitude of 0.006 mag. To verify the detection of both periods, we have also used DFT/CLEAN to search for multiple periods. Figure 22 shows the window power spectrum, the raw DFT power spectrum of the light curve, and the power spectrum after using CLEAN. Using DFT/CLEAN we find two strong period detections at 0.941 ± 0.011 days and 1.174 ± 0.013 days. In figure 23 we show the original light curve phased at the orbital period of the system, the out of eclipse points phased at 0.941 days, the residual light curve after subtracting the above period phased at 1.174 days, and the full light curve after subtracting a double sinusoid fit to the out of eclipse points. The model is subtracted through the eclipses, though this is technically incorrect. We adopt the DFT/CLEAN periods for the rest of the discussion.

The additional periods are most likely not the rotation periods of the two binary components. The time-scale for the synchronization of rotation periods with the orbital period is much shorter than the time-scale for the circularization of the orbit (Zahn 1977). Since the orbit appears to be circular (see below), we expect that it should also be synchronized. We will show that the additional periods are most likely due to one or both of the stars being a γ -Doradus type pulsator.

We will now determine the physical masses and radii of the components of this binary system. To do this we will combine radial velocity curves with our light curve.

This binary was among the sources that we obtained spectra for with Hectochelle. The spectroscopic classification procedure discussed in Paper I yields a temperature of $T_{eff} = 6600 \pm 400$ K, and $v \sin i = 21.5 \pm 0.7$ km/s, these values are an average of the two stars. The metallicity is unconstrained so we assume solar metallicity. Only the spectra for the first two nights are used in the classification since the two components were not well separated in the last two nights; classifying spectra from the last two nights yields an artificially high value for $v \sin i$. For the cluster reddening of $E(B - V) = 0.219$ (Paper I), the expected color of the system is $B - V = 0.64 \pm 0.1$ which is consistent with the observed value of $B - V = 0.594$.

We combine the spectra from each of the four usable nights and calculate the cross-correlation as a function of radial velocity (RV) with *xcsao* using the best template from the classification procedure. The cross-correlation plots show two clear peaks, indicating that we do detect the system as a double-lined spectroscopic binary. We then use the TwO-

Dimensional CORrelation algorithm (TODCOR; Zucker and Mazeh 1994) to determine the velocities for each component. We use the same template for both stars as the nearly equal depth eclipses means that the stars have similar surface temperatures. Table 5 lists the radial velocity and light ratio measurements from the spectra. The average light ratio in the RV31 filter is $L_2/L_1 = 0.992 \pm 0.025$.

To combine the radial velocity curves with the light curve we need to improve the period that is derived from the light curve. To do this we fit a zero-eccentricity orbital solution to the radial velocity curves, assuming the period determined from the light curve, and allowing for a shift in phase. From the phase shift we calculate a single “observed” primary eclipse time at the epoch of the RV observations. We then determine eclipse minimum times from the light curve using the Detached Eclipsing Binary Light curve fitter (DEBiL; Devor 2005) and fit for the ephemeris using the equation:

$$T_{min} = HJD_0 + nP. \quad (7)$$

Here T_{min} is the observed minimum time, HJD_0 is the reference primary eclipse epoch, P is the orbital period and n is the eclipse number. We find $HJD_0 = 2453724.5306 \pm 0.0004$ and $P = 2.19258 \pm 0.00004$ days. The observed eclipse timing measurements are listed in table 6. We include secondary eclipses in the fit and assume zero eccentricity, which we justify below.

Using the above ephemeris, we fit a zero-eccentricity orbit to the RV curves finding $K_1 = 118.3 \pm 1.3$ km/s, $K_2 = 118.3 \pm 1.3$ km/s and $\gamma = 5.3 \pm 0.7$ km/s. The mass ratio is thus $q = 1.00 \pm 0.01$, so the two components have equal mass to within the precision of our observations. This is another example of a twin binary star system (Pinsonneault and Stanek 2006). The systemic radial velocity γ is more than 3σ below the mean cluster value of 9.2 ± 1.4 km/s (Paper I). Figure 24 shows the radial velocity observations with the best fit orbit.

Since the system is well detached, we model the light curve using the JKTEBOP program (Southworth, Maxted, & Smalley 2004; Southworth et al. 2004) which is based on the Eclipsing Binary Orbit Program (EBOP; Popper and Etzel 1981; Etzel 1981; Nelson and Davis 1972), but includes more sophisticated minimization and error analysis routines. We assume a linear limb darkening law, adopting $u = 0.564$ for both the primary and secondary stars. This coefficient is appropriate for the the r filter with $T_{eff} = 6600$ K, $\log(g) = 4.5$ and $[M/H] = 0.0$ (Claret 2004). We use a gravity darkening exponent of 1.0, which is the value expected for a radiative envelope star, though the effect is negligible in this system. The resulting parameters are given in table 7, where the listed errors are the 1σ errors from 100 Monte Carlo simulations. Southworth et al. (2005) have shown that the Monte Carlo routine in JKTEBOP provides robust error estimates, though we note that uncertainties in the limb darkening and reflection laws are not included in the Monte Carlo simulations. In conducting the simulations we set the error on each point in the light curve equal to 3.9

mmag, which is the RMS of the residual from the best fit. The best fit model to the light curve is shown in figure 25.

The ratio of the radii, k , is poorly constrained from the light curve. A better constraint could be obtained by including the spectroscopic constraint on the luminosity ratio, however since the spectra were obtained over a significantly different wavelength range from the light curve, including this constraint is not straightforward and beyond the scope of this paper.

To put a limit on the eccentricity of the system, we have also fit the light curve allowing $e \cos \omega$ and $e \sin \omega$ to vary. We find $e = 0.003 \pm 0.01$, which is consistent with a circular orbit. The error is determined from 100 Monte Carlo simulations. The 3σ upper bound on the eccentricity is $e < 0.03$. We have also attempted varying the third light contribution to the system, finding $L_3 = 0.06 \pm 0.14$ which is consistent with zero, though poorly constrained.

Combining the parameters determined from the RV curves with the parameters determined from the light curve, we find the following masses and radii for the stars: $M_P = 1.58 \pm 0.04 M_\odot$, $R_P = 1.39 \pm 0.07 R_\odot$, $M_S = 1.58 \pm 0.04 M_\odot$, and $R_S = 1.38 \pm 0.07 R_\odot$. The errors in the masses are dominated by the uncertainties in the velocity semi-amplitudes, while the errors in the radii are dominated by the large uncertainty in R_S/R_P .

In figure 26 we plot the age-metallicity χ^2 contours for the eclipsing binary system. To calculate χ^2 at each age/metallicity point we use the Yale-Yonsei version 2 isochrones (Y2 Demarque et al. 2004) and find the pair of masses which minimize

$$\chi^2 = \frac{(K_P - K_{P, \text{isoc}}(M_P, P, \sin i))^2}{\sigma_{K_P}^2} + \frac{(K_S - K_{S, \text{isoc}}(M_S, P, \sin i))^2}{\sigma_{K_S}^2} + \frac{(\alpha - \alpha_{\text{isoc}}(M_P, M_S, P))^2}{\sigma_\alpha^2} + \frac{(k - k_{\text{isoc}}(M_P, M_S))^2}{\sigma_k^2} + \frac{(T_{\text{ave}} - T_{\text{ave, isoc}}(M_P, M_S))^2}{\sigma_T^2} \quad (8)$$

where the “isoc” subscript denotes values calculated from the isochrones using the trial masses (M_P and M_S) and the measured orbital period (P) and $\sin i$, $\alpha = (R_P + R_S)/a$, $k = R_S/R_P$, and T_{ave} is the average temperature of the two stars. The contours in figure 26 show the 68.3%, 95.4% and 99.7% confidence levels. The point shows the values for the cluster using the Y2 isochrones (see Paper I). The binary system is younger and has a lower metallicity than the cluster.

Figure 27 shows the observed masses and radii of the components together with the expected relation for the cluster from the Y2 isochrones and the relation for $[M/H] = -0.25$ and an age of 100 Myr. The stars appear to have radii that are too small given their masses for them to have the metallicity and age of the cluster.

The individual r magnitudes of the stars are $r_p = 15.53$ and $r_s = 15.55$. As we stated

at the beginning of this subsection, the expected masses for the stars if the system were a member of the cluster would be $M_p = M_s = 1.18 \pm 0.04M_\odot$, with an uncertainty dominated by the systematic uncertainty in the $M - r$ relation. The observed masses are $\sim 7\sigma$ above the expected masses, this together with the metallicity discrepancy (see figure 26), and the $\sim 3\sigma$ discrepancy between the systemic velocity and the mean RV of the cluster stars leads us to conclude that the system is most likely not a member of the cluster, and is instead located in the background galactic disk.

Finally, we return to the nature of the non-eclipse variability seen in the light curve. γ Doradus type variables are early F-type main sequence stars that have periods in the range of 0.4 – 3 days, amplitudes of a few percent and typically oscillate in multiple frequencies (Krisciunas 1998; Kaye et al. 1999). The instability strip for this type of variable extends from 7200 – 7550 K on the zero-age main sequence (ZAMS) and from 6900 – 7400 K near the end of the main sequence phase (Dupret et al. 2004). The periods and amplitudes of the non-eclipse variations are consistent with one or both of the stars being a γ Doradus pulsator. The spectroscopic temperature is slightly lower than, though consistent with, the instability strip for this type of pulsator.

As seen in figure 26, the eclipsing binary components appear to be relatively young (< 700 Myr at 3σ , < 200 Myr at 1σ). This is consistent with some indications that the γ Doradus phenomenon is restricted to stars with ages < 250 Myr (Krisciunas 1998), though there are potentially a few γ Doradus variables as old as 1 Gyr that have been discovered (Pepper and Burke 2006). To our knowledge, V1345 is only the second γ Doradus variable found in an eclipsing binary, the other system being VZ CVn (İbanoğlu et al. 2007). These systems are particularly interesting since the geometry allows for the direct determination of the masses and radii of the stars, and with precise photometry it may be possible to use the eclipses to aid in identifying the pulsation modes (Riazi and Abedi 2006).

6.5. Detached Eclipsing Binary V1002

Based on its photometry, the detached eclipsing binary V1002 is a candidate cluster member. V1002 matches to 2mass05523843+3223296, it has an orbital period of 5.496 ± 0.18 days, a primary eclipse epoch of $HJD_0 = 2453725.6977$, and photometry $B - V = 1.591$, $V = 19.428$, $g - r = 1.61$, $r - i = 0.93$, $r = 18.73$, $J - K_S = 0.695$, $H - K_S = 0.137$, and $K_S = 15.289$. If the system is a member of the cluster, its primary would have a mass of $0.6 < M < 0.7M_\odot$ based on the r magnitude of the system. We will now demonstrate that the components of this system likely have masses of $\sim 0.6M_\odot$ and may very well be members of the cluster.

This system shows out of eclipse variations with a peak-to-peak amplitude of 0.028 mag. Since the maximum of this variation does not occur at either of the quadrature points or near the eclipses, and since the system is well detached, the variation is most likely due to spots on one of the stars rather than due to proximity effects. This confirms that at least one of the stars has a rotation period synchronized to the orbital period. The primary and secondary eclipses occur 0.5 apart in phase, so it appears that the system is also circularized.

Before fitting an eclipse model to the light curve, we first remove the out of eclipse variation using a sinusoid. Assuming the cluster reddening and assuming all the light comes from the primary component, we estimate the temperature of the primary is ~ 5000 K from the $J - K_S$ and $H - K_S$ colors, for which the r quadratic limb darkening coefficients are $a = 0.538$, $b = 0.199$ (Claret 2004). Using JKTEBOP, we fit the light curve assuming zero eccentricity and find the parameters listed in table 8. As before we estimate the parameter errors using 100 Monte Carlo simulations taking the error at each observation to be 8.0 mmag. In this case we refine the period and primary eclipse epoch using JKTEBOP. We find that it is necessary to include a significant amount of third light ($L_3 = 0.266 \pm 0.006$) in the fit, though it is unclear if this is an artifact of not correctly modelling the spot through the eclipses. The resulting fractional radii for the primary and secondary stars are $R_P/a = 0.0439 \pm 0.0003$ and $R_S/a = 0.0416 \pm 0.0004$. Figure 28 shows the best fit model to the light curve.

To estimate the masses of the component stars we use Kepler’s third law and the mass-radius relation for low-mass stars. Assuming a power-law mass-radius relation of the form $M = M_0(R/R_\odot)^b$, the mass of each component is given by:

$$M_{P,S} = M_0 \left(\frac{R_{P,S}}{a} \right)^b \left(74.471 \frac{M_0}{M_\odot} \left(\frac{P}{1 \text{ day}} \right)^2 \left(\left(\frac{R_P}{a} \right)^b + \left(\frac{R_S}{a} \right)^b \right) \right)^{b/(3-b)}. \quad (9)$$

For the mass-radius relation we use the double-lined detached eclipsing binary data given in Ribas (2006) to find $(M/M_\odot) = 1.04(R/R_\odot)^{1.08}$.

Using eq. 9 we find component masses of $M_P \sim 0.61M_\odot$, and $M_S \sim 0.57M_\odot$. The mass of the primary is thus close to what we would expect based on the r magnitude of the system if the stars were members of the cluster. The individual magnitudes of the two component stars are $r_P \sim 19.5$ and $r_S \sim 20.1$, with a third component having $r_3 \sim 20.4$. The magnitude difference of 0.59 ± 0.03 between the primary and secondary stars is quite a bit larger than the value of 0.3 that one would expect from the estimated masses (see the mass- r magnitude relation in Paper I). However, given that we do not properly model the spots on the stars through the eclipses, and that we do not have radial velocity data to confirm the masses, the discrepancy may simply be an artifact of our modelling.

We have shown that the stars likely have masses of $\sim 0.6M_{\odot}$ and may very well be members of the cluster. The system is therefore interesting for follow-up as only ~ 6 double-lined detached eclipsing binary systems with main sequence stars smaller than the components in this system are known, and the models for these stars are known to be in error by 5 – 20% (Ribas 2006). If the system proves to be a member of the cluster, then the additional constraints on its age, metallicity and apparent distance modulus would make the system particularly useful in testing low mass stellar models. The downside though to any follow-up is that with $V \sim 19.4$, a significant amount of large telescope time would be needed to obtain its radial velocity curve. Note that the expected semi-amplitude of the radial velocity curve is ~ 60 km/s.

7. Conclusion

In this paper we have identified 1395 new variable stars in the field of M37. Approximately 500 of these variables are F-M main sequence cluster members; for these stars the variability is due to rotation coupled with significant surface brightness inhomogeneities. This data set is significantly larger than any other set of stellar rotation periods for a cluster that is $\gtrsim 500$ Myr old and will thus provide a unique window on the rotation of lower main sequence stars. We argue that many of the other variable stars are young, rapidly rotating main sequence stars in the galactic disk by showing that the amplitude of these variables is anti-correlated with the Rossby number.

We have used the W UMa eclipsing binaries and fundamental mode δ -Scuti found by this survey to investigate the relation between distance and extinction along the line of sight, and have shown that the extinction apparently cuts off at nearly twice the scale height of the disk.

Finally, we have analyzed a few particularly interesting variable stars including a previously identified multi-mode pulsator which we argue to be a hybrid γ -Doradus/ δ -Scuti, a white dwarf or subdwarf B star that shows pulsation like variations that are substantially longer in period and greater in amplitude than typical, a possible quiescent cataclysmic variable, a DEB with at least one γ -Doradus pulsating component, and a low mass DEB that is a possible cluster member. We have combined radial velocity and light curves to obtain a physical solution for the DEB+ γ -Doradus system.

This research has made use of the SIMBAD database, operated at CDS, Strasbourg, France. We are grateful to C. Alcock for providing partial support for this project through his NSF grant (AST-0501681). Funding for M. Holman came from NASA Origins grant

NNG06GH69G. We would like to thank G. Torres for help with running the eclipsing binary analysis software and for helpful comments, G. Fűrész and A. Szentgyorgyi for help in preparing the Hectochelle observations, S. Meibom for help with the stellar classification, and the staff of the MMT, without whom this work would not have been possible. We would also like to thank the MMT TAC for awarding us a significant amount of telescope time for this project.

A. The VARTOOLS Program

In conducting the research described in this paper we have developed software to perform a number of common analysis routines on a set of light curves. The program is called VARTOOLS and we release it to the community². The program reads in a light curve, or a set of light curves, in ascii format and performs a series of commands on them; it is designed to run the light curves through a pipeline of routines.

At the time of writing the commands that can be run include the period finding routines discussed in §3, routines to fit a Fourier series to light curves, and routines to linearly decorrelate light curves against generic signals. This is not an exhaustive list; a full description of the program can be found on the website.

REFERENCES

- Alard, C. & Lupton, R. 1998, *ApJ*, 503, 325
- Alard, C. 2000, *A&AS*, 144, 363
- Binnendijk, L. 1960, *AJ*, 65, 385
- Brown, W. R., Geller, M. J., Kenyon, S. J., Kurtz, M. J., Bromley, B. C. 2007, *ApJ*, in press, arXiv:0709.1471 [astro-ph]
- Claret, A. 2004, *A&A*, 428, 1001
- Córsico, A. H., Althaus, L. G., & Miller Bertolami, M. M. 2006, *A&A*, 461, 1095
- Demarque, P., Woo, J.-H., Kim, Y.-C., & Yi, S. K. 2004, *ApJS*, 155, 667

²<http://www.cfa.harvard.edu/~jhartman/vartools>

- Devor, J. 2005, *ApJ*, 628, 411
- Duerbeck, H. W. 1996, in *Light Curves of Variable Stars, A Pictorial Atlas*, ed. C Sterken & C Jaschek (Cambridge: Cambridge University Press), 141
- Dupret, M.-A., Grigahcène, A., Garrido, R., Gabriel, M., & Scufflaire, R. 2004, *A&A*, 414, L17
- Efron, B., & Petrosian, V. 1992, *ApJ*, 399, 345
- Efron, B., & Petrosian, V. 1999, *JSTOR*, 94, 447, p. 824-834
- Etzel, P. B. 1981, *NATO ASI*, p. 111
- Frandsen, S., & Arentoft, T. 1998, *A&A*, 333, 524
- Girardi, L., Grebel, E. K., Odenkirchen, M., Chiosi, C. 2004, *A&A*, 422, 205
- Green, E. M., et al. 2003, *ApJ*, 583, L31
- Hartman, J. D., Bakos, G., Stanek, K. Z., & Noyes, R. W. 2004, *AJ*, 128, 1761
- Hartman, J. D., et al. 2007, *ApJ*, submitted, arXiv:0709.3063 [astro-ph] (Paper I)
- İbanoglu, C., Taş, G., Sipahi, E., & Evren, S. 2007, *MNRAS*, 376, 573
- Irwin, J., Aigrain, S., Hodgkin, S., Irwin, M., Bouvier, J., Clarke, C., Hebb, L., & Moraux, E. 2006, *MNRAS*, 370, 9541
- Irwin, J., et al. 2007, *MNRAS*, 377, 741
- Kalirai, J. S., Ventura, P., Richer, H. B., Fahlman, G. G., Durrell, P. R., D'Antona, F., & Marconi, G. 2001, *AJ*, 122, 3239
- Kang, Y. B., Kim, S.-L., Rey, S.-C., Lee, C.-U., Kim, Y. H., Koo, J.-R., & Jeon, Y.-B. 2007, *PASP*, 119, 239
- Kaye, A. B., Handler, G., Krisciunas, K., Poretti, E., & Zerbi, F. M. 1999, *PASP*, 111, 840
- Kilkenny, D., O'Donoghue, D., Reed, M. D., Hambly, N., & McGillivray, H. 2006, *BaltA*, 15, 317
- King, H. 2006, *CoAst*, 148, 28
- Kiss, L. L., Szabó, Gy. M., Sziládi, K., Fűrész, G., Sárneczky, K., & Csák, B. 2001, *A&A*, 376, 561

- Kovács, G., Zucker, S. & Mazeh, T. 2002, *A&A*, 391, 369
- Kovács, G., Bakos, G., & Noyes, R. W. 2005, *MNRAS*, 356, 557
- Krisciunas, K. 1998, in *IAU Symp. 185, New Eyes to See Inside the Sun and Stars*, ed. F.-L. Deubner, J. Christensen-Dalsgaard, & D. Kurtz (Dordrecht: Kluwer), 339
- Liu, Q.-Y., & Yang, Y.-L. 2003, *ChJAA*, 3, 142
- Lomb, N. R. 1976, *A&SS*, 39, 447
- McLeod, B. A., Conroy, M., Gauron, T. M., Geary, J. C., & Ordway, M. P. 2000, in *Proc. International Conference on Scientific Optical Imaging, Further Developments in Scientific Optical Imaging*, ed. M. Bonner Denton (Cambridge: Royal Soc. Chemistry), 11
- McNamara, D. H., Madsen, J. B., Barnes, J., & Ericksen, B. F. 2000, *PASP*, 112, 202
- Messina, S., Rodonò, M., & Guinan, E. F. 2001, *A&A*, 366, 215
- Moehler, S., Heber, U., & Rupprecht, G. 1997, *A&A*, 319, 109
- Nelson, B., & Davis, W. D. 1972, *ApJ*, 174, 617
- Nilakshi, & Sagar, R. 2002, *A&A*, 381, 65
- Noyes, R. W., Hartmann, L. W., Baliunas, S. L., Duncan, D. K., & Vaughan, A. H. 1984, *ApJ*, 279, 763
- O’Connell, D. J. K. 1951, *Pub. Riverview College Obs.*, 2, 85
- Pepper, J., & Burke, C. J. 2006, *AJ*, 132, 1177
- Pinsonneault, M. H., & Stanek, K. Z. 2006, *ApJ*, 639L, 67
- Pont, F., Zucker, S., & Queloz, D. 2006, *MNRAS*, 373, 231
- Popper, D. M., & Etzel, P. B. 1981, *AJ*, 86, 102
- Press, W. H. & Rybicki, G. B. 1989, *ApJ*, 338, 277
- Press, W. H., Teukolsky, S. A., Vetterling, W. T. & Flannery, B. P. 1992, *Numerical Recipes in C*, 2nd ed. (New York: Cambridge University Press)
- Radick, R. R., Thompson, D. T., Lockwood, G. W., Duncan, D. K., & Baggett, W. E. 1987, *ApJ*, 321, 459

- Riazi, N., & Abedi, A. 2006, *New Astron.*, 11, 514
- Ribas, I. 2006, *Ap&SS*, 304, 89
- Roberts, D. H., Lehár, J., & Dreher, J. W. 1987, *AJ*, 93, 4
- Robin, A. C., Reylé, C., Derrière, S., & Picaud, S. 2003, *A&A*, 409, 523
- Rucinski, S. M., & Duerbeck, H. W. 1997, *PASP*, 109, 1340
- Scargle, J. D. 1982, *ApJ*, 263, 835
- Schlegel, D. J., Finkbeiner, D. P., & Davis, M. 1998, *ApJ*, 500, 525
- Schmidt-Kaler, T. 1982, in “Landolt-Bornstein: Numerical data and Functional Relationships in Science and Technology,” Vol 2b, eds. Schiefers, K., Voigt, H. H. (Berlin: Springer).
- Schwarzenberg-Czerny, A. 1991, *MNRAS*, 253, 198
- Schwarzenberg-Czerny, A. 1996, *ApJ*, 460, 107
- Shaw, J. S. 1994, *Mem. S. A. It.*, 65, 1
- Skrutskie, M. F., et al. 2006, *AJ*, 131, 1163
- Southworth, J., Maxted, P. F. L., & Smalley, B. 2004, *MNRAS*, 351, 1277
- Southworth, J., Zucker, S., Maxted, P. F. L., & Smalley, B. 2004, *MNRAS*, 355, 986
- Southworth, J., Smalley, B., Maxted, P. F. L., Claret, A., & Etzel, P. B. 2005, *MNRAS*, 363, 529
- Sterken, C., & Jerzykiewicz, M. 1993, *SSRv*, 62, 95
- Szentgyorgyi, A. H., Cheimets, P., Eng, R., Fabricant, D. G., Geary, J. C., Hartmann, L., Pieri, M. R., & Roll, J. B. 1998, in *Proc. SPIE 3355, Optical Astronomical Instrumentation*, ed. S. D’Odorico, 242-252
- Tamuz, O., Mazeh, T., & Zucker, S. 2005, *MNRAS*, 356, 1466
- Tsai, W. 1990, *Biometrika*, 77, 169
- Zahn, J.-P. 1977, *A&A*, 57, 383
- Zucker, S., & Mazeh, T. 1994, *ApJ*, 420, 806

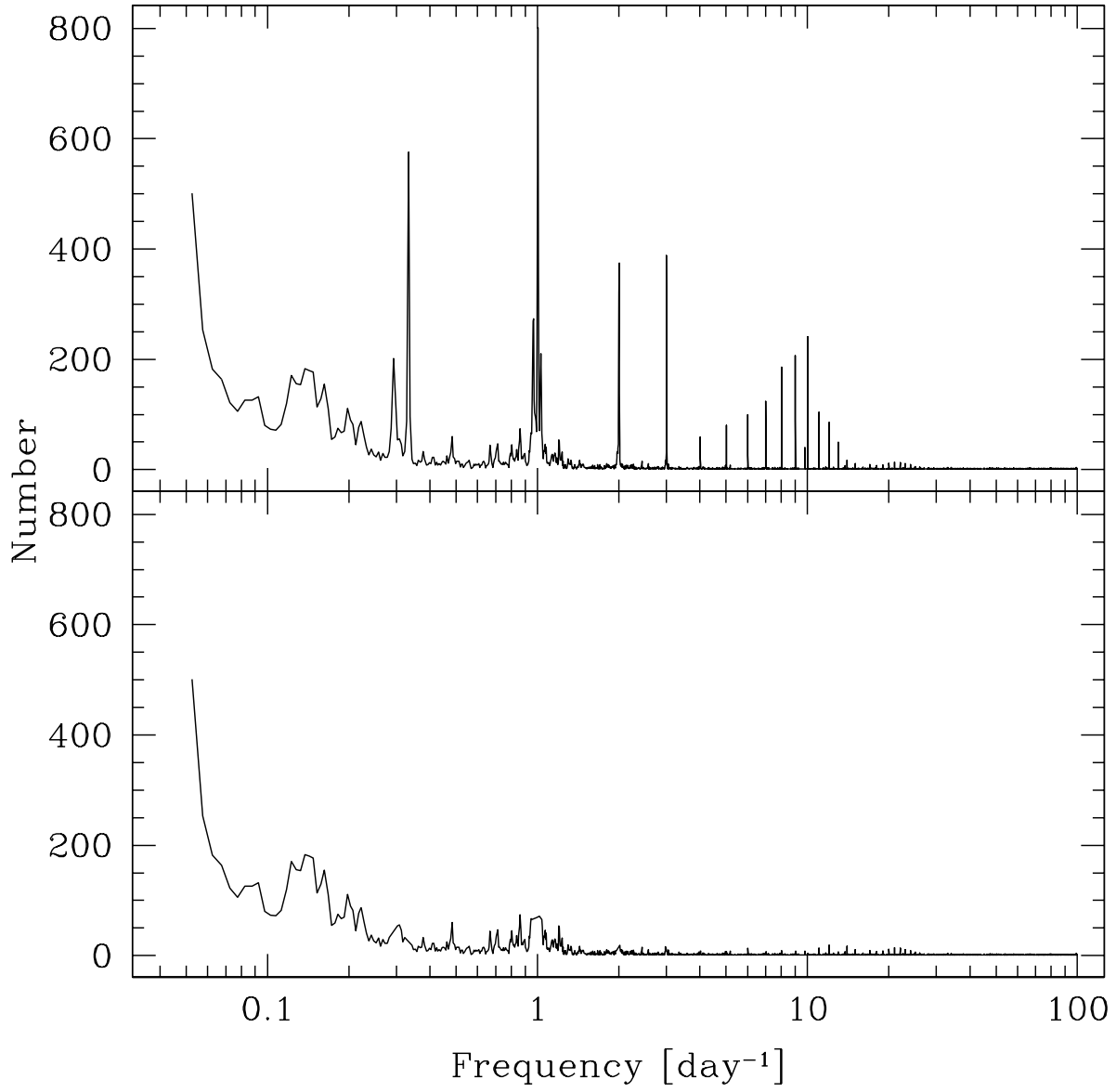


Fig. 1.— Histogram of peak frequencies in the Lomb-Scargle periodograms of all light curves. The top panel shows the histogram before removing bad frequencies (seen as spikes in the periodogram), the bottom shows the histogram after removing them.

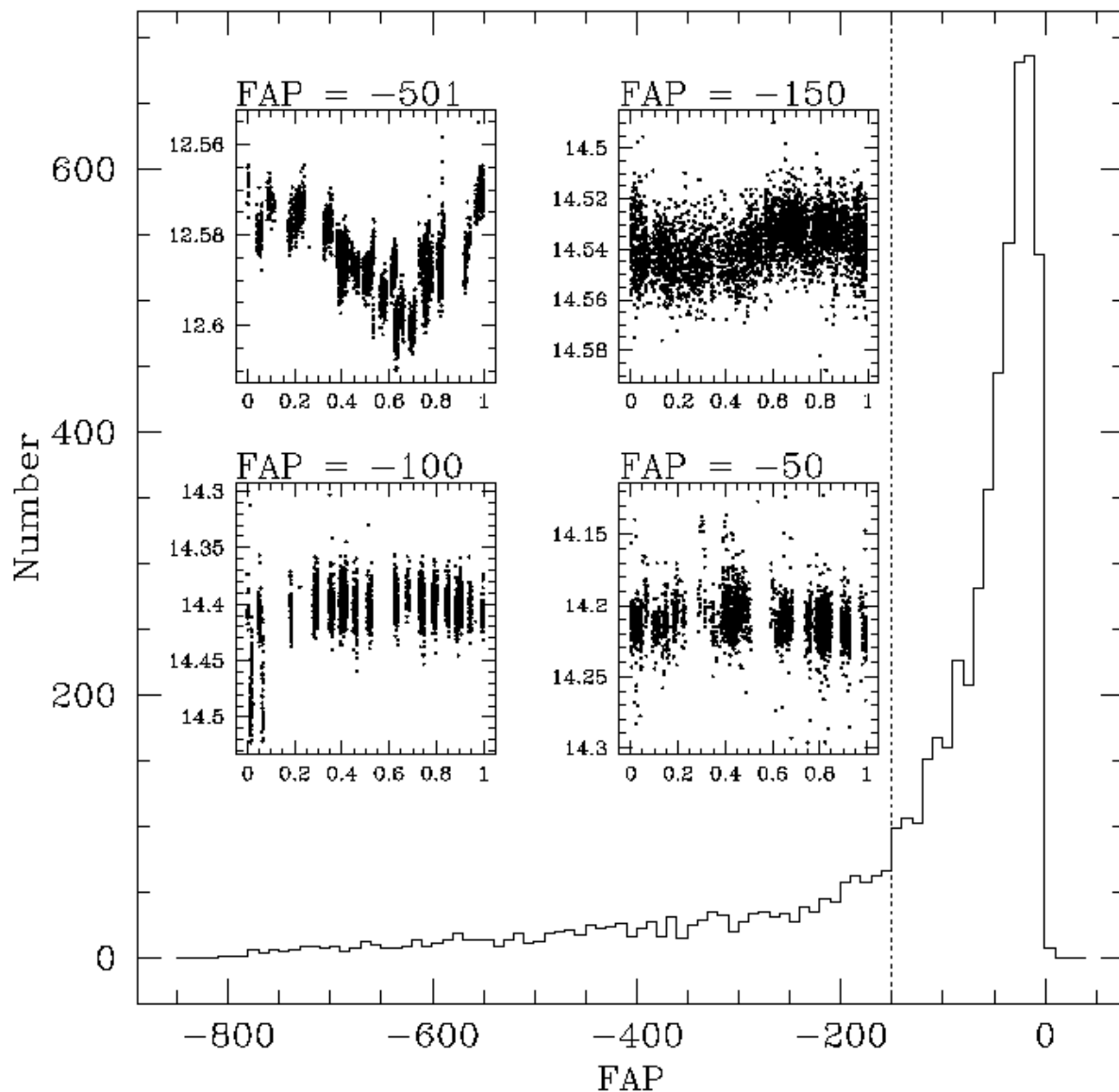


Fig. 2.— Histogram of the logarithm of the formal false alarm probability values from the Lomb-Scargle period finding algorithm. Example phased light curves at a range of FAP values are shown. The units on the inset plots are phase for the x-axis and r magnitude for the y-axis. We select stars with $FAP < -150$ as variables. The dotted line shows this selection.

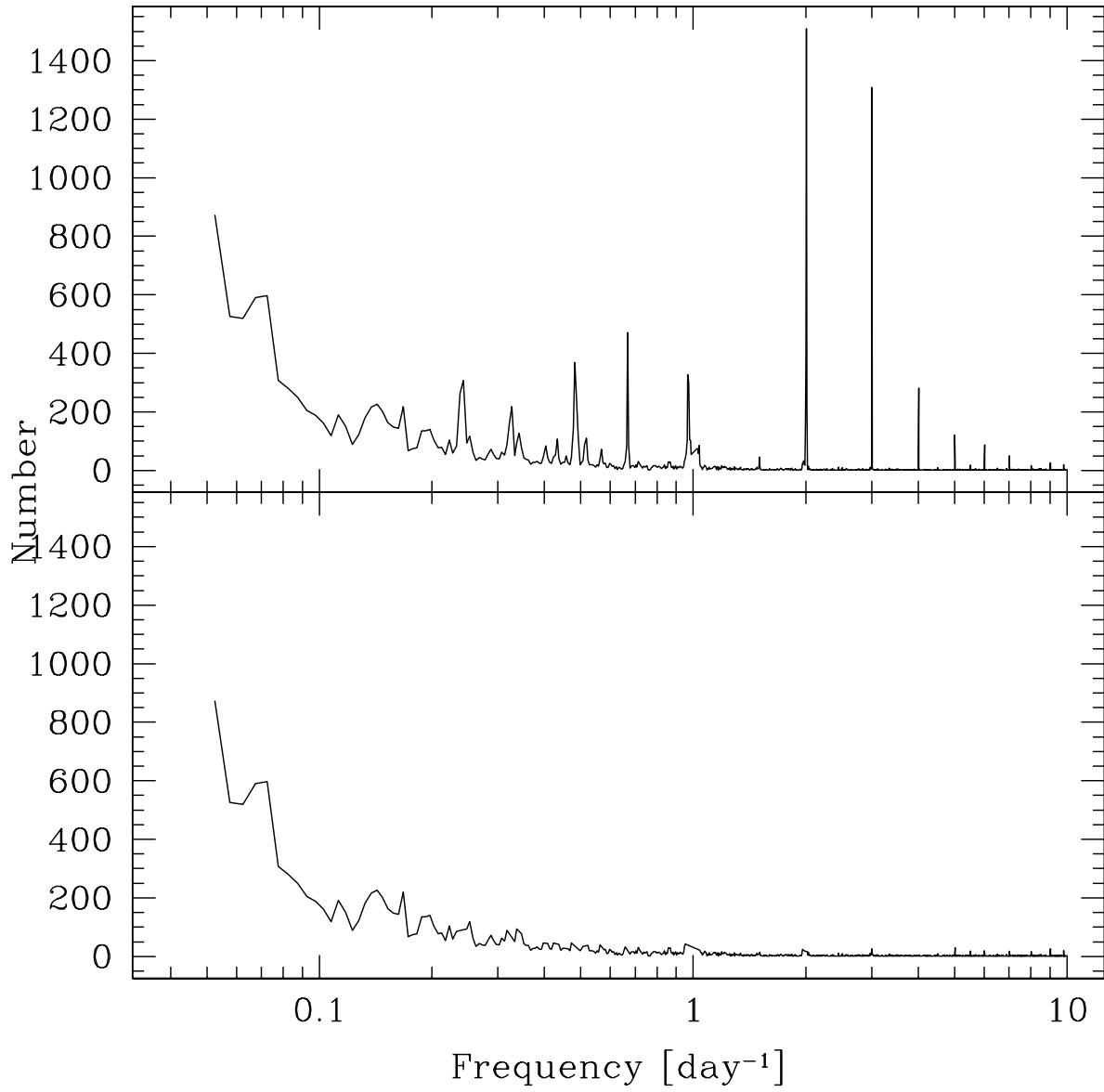


Fig. 3.— Same as figure 1, this time shown for AoV.

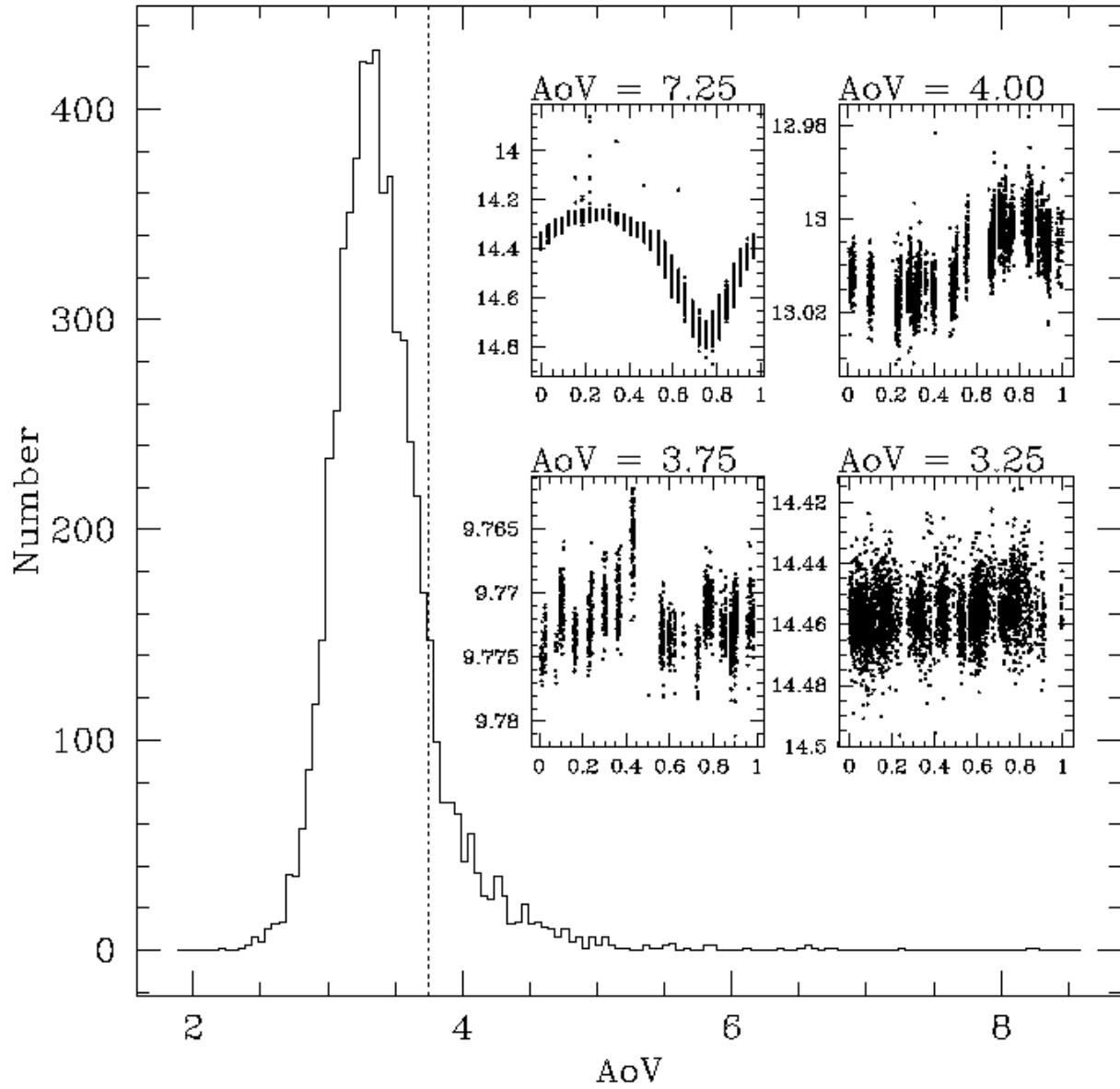


Fig. 4.— Same as figure 2, here we plot the histogram of AoV. The selection criterion is $AoV > 3.75$.

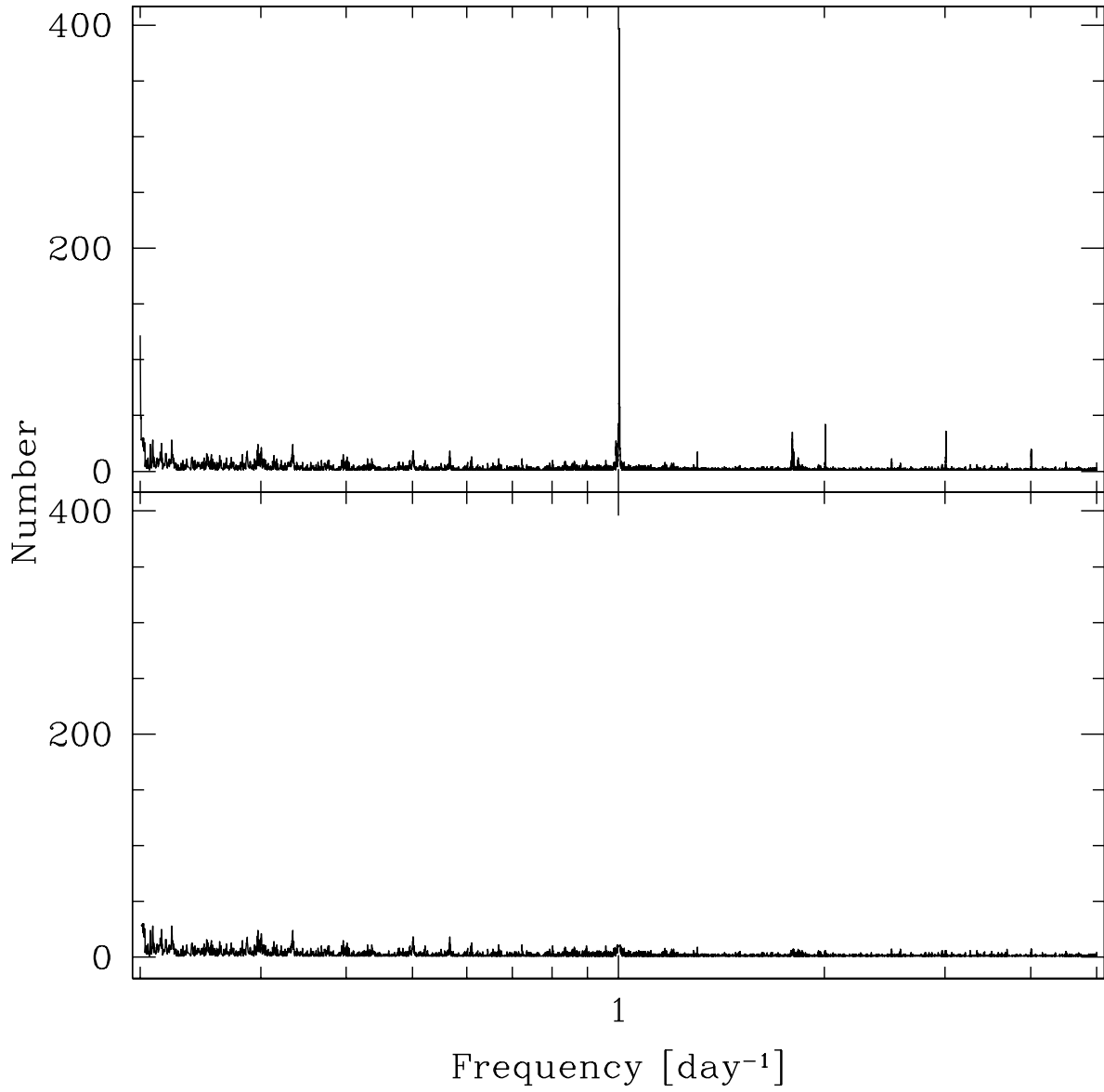


Fig. 5.— Same as figure 1, this time shown for BLS.

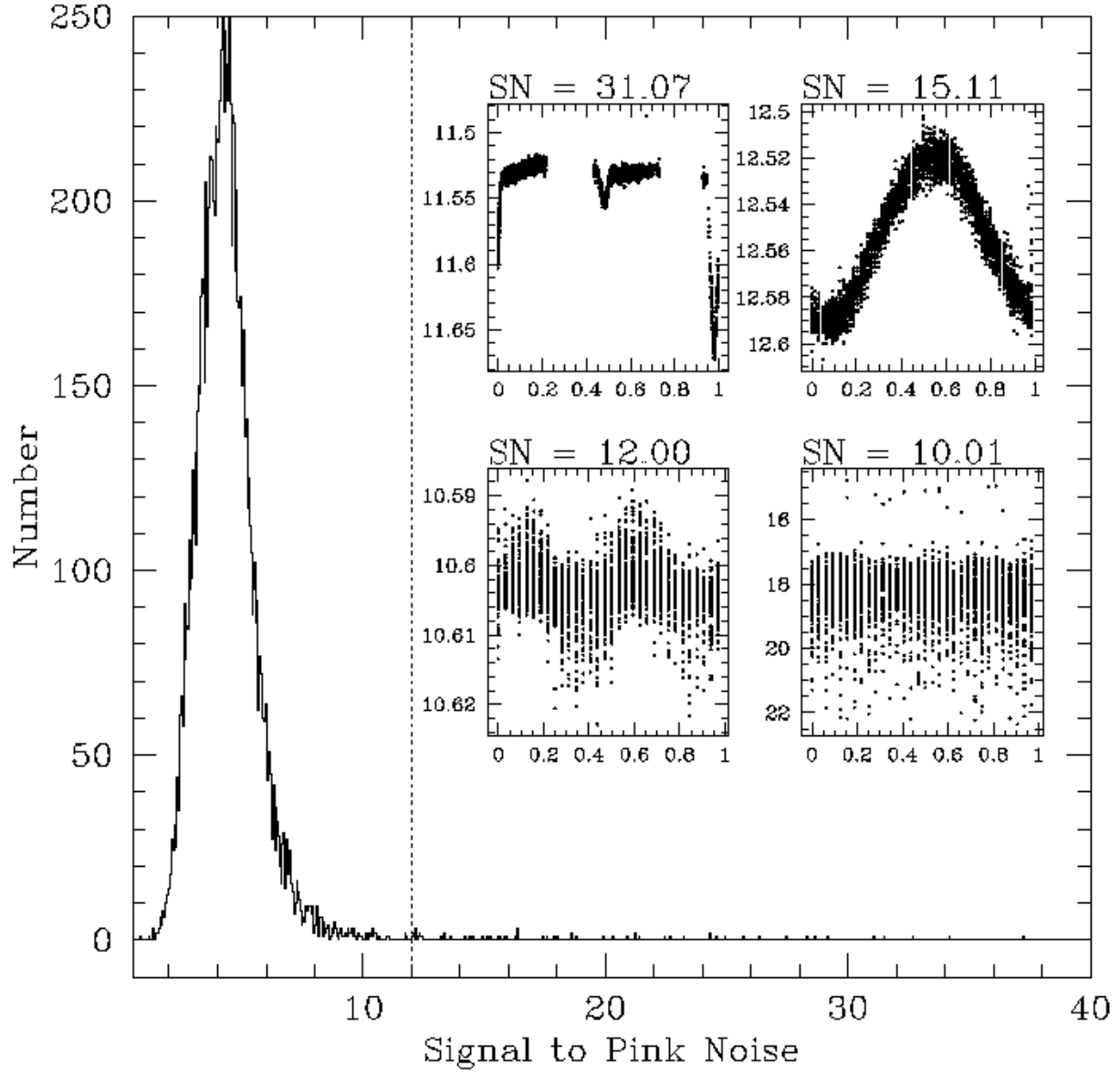


Fig. 6.— Same as figure 2, this time shown for BLS. The selection criterion is $SN > 12.0$.

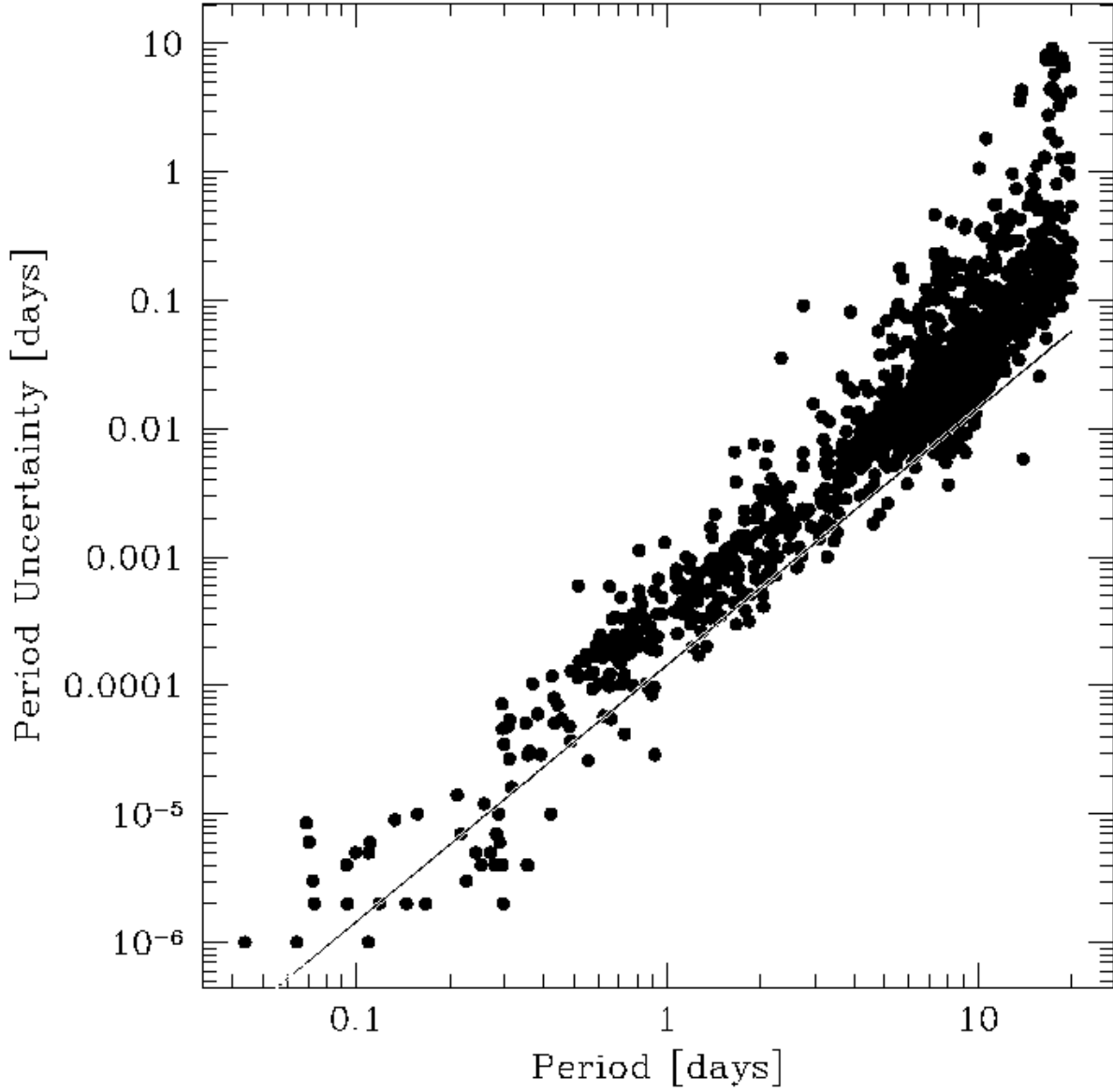


Fig. 7.— The uncertainty on the variable star periods as a function of period. The solid lines shows the expected relation for a signal to noise of 10 and a residual correlation time-scale of 30 minutes.

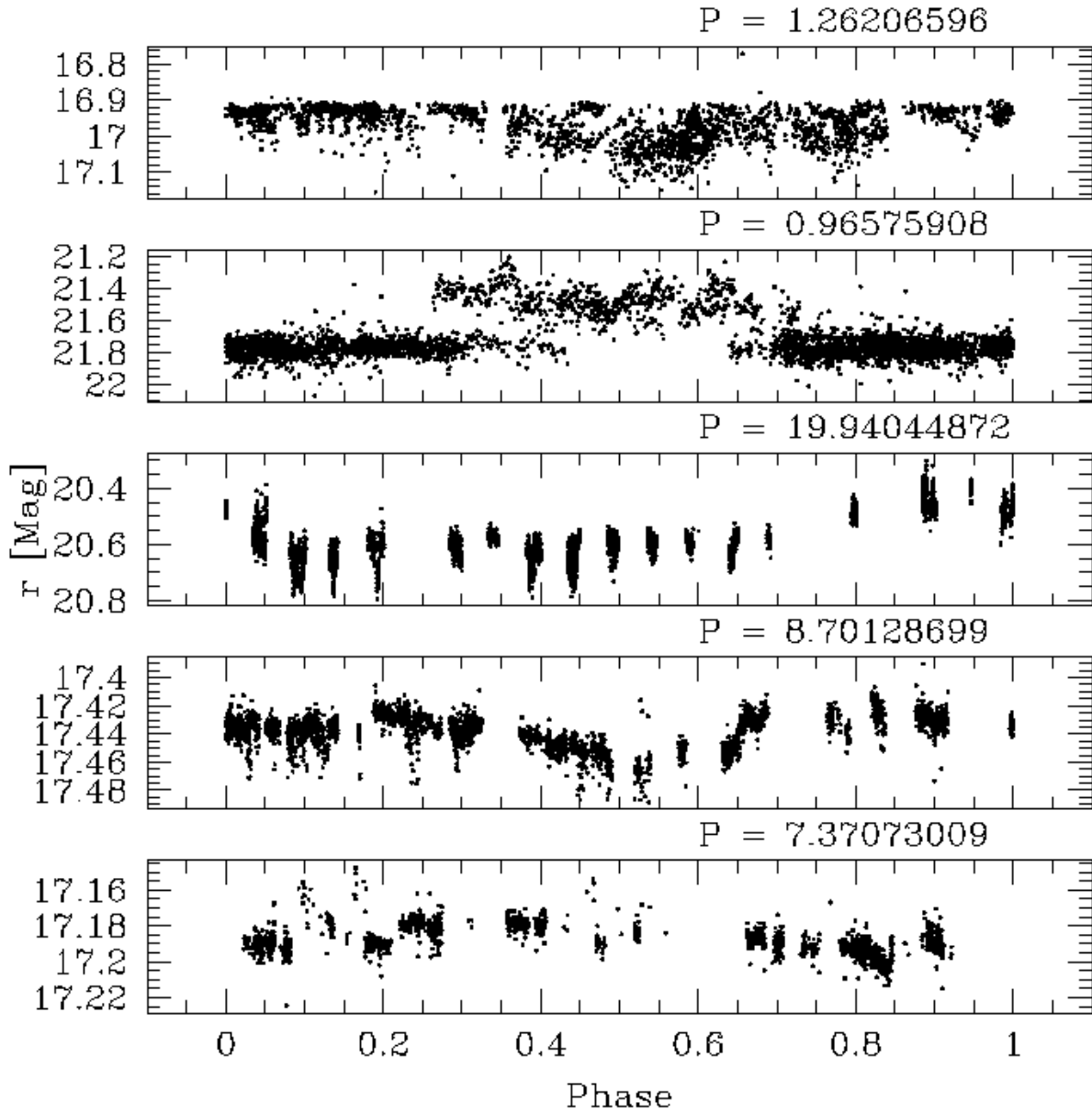


Fig. 8.— Examples of candidate variable star light curves which were rejected by eye. The listed period is the value returned by LS and is in days.

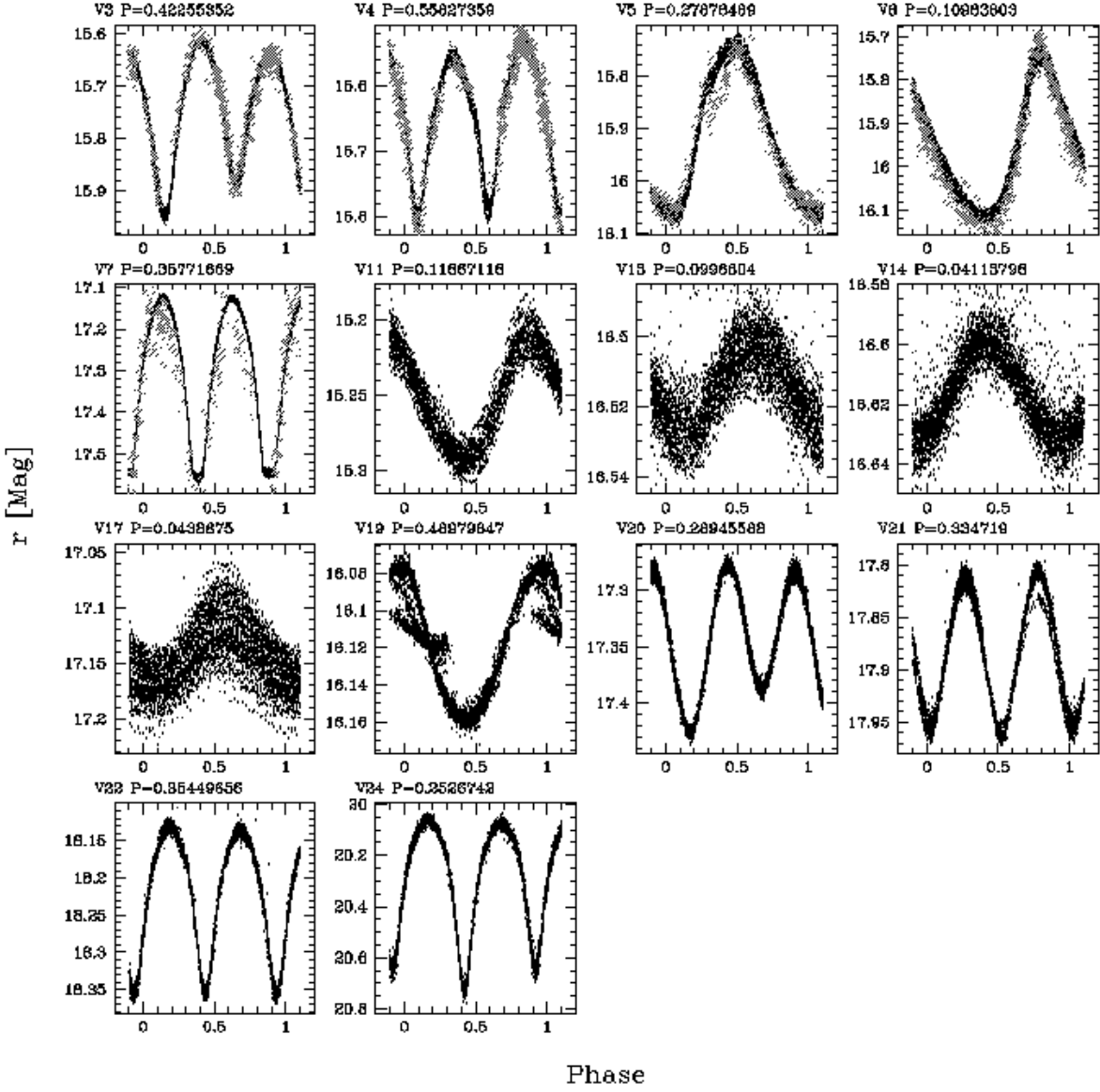


Fig. 9.— Light curves of 14 previously identified variables that we match to. For variables V3-V7 we overplot the R_c published photometry from Kiss et al. (2001) in gray. The Kiss et al. (2001) photometry has been shifted by an offset to match up with our data.

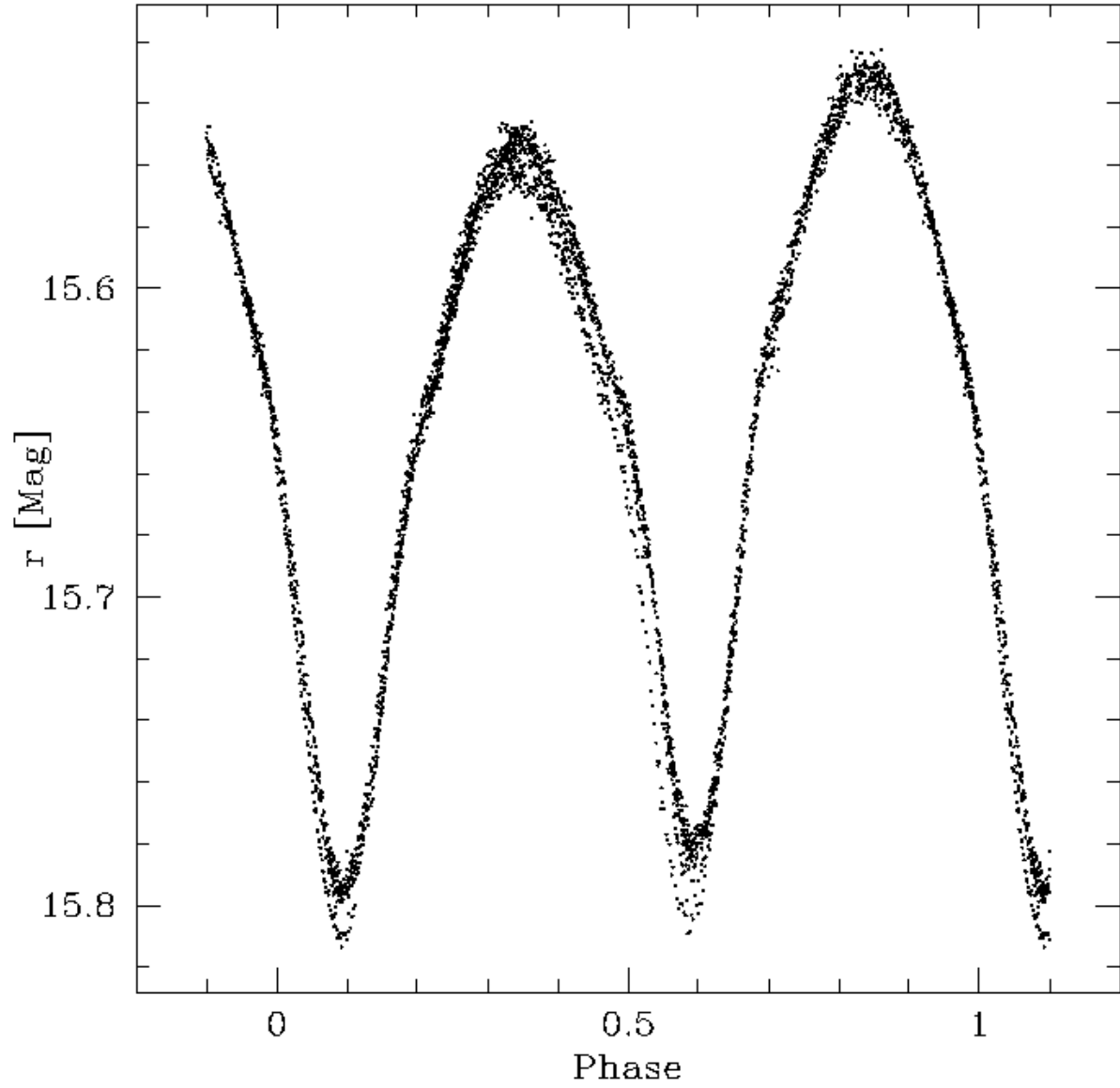


Fig. 10.— Phased light curve of the contact eclipsing binary V4. The light curve exhibits a pronounced O’Connell effect and also shows evidence for variations of ~ 0.01 mag between cycles.

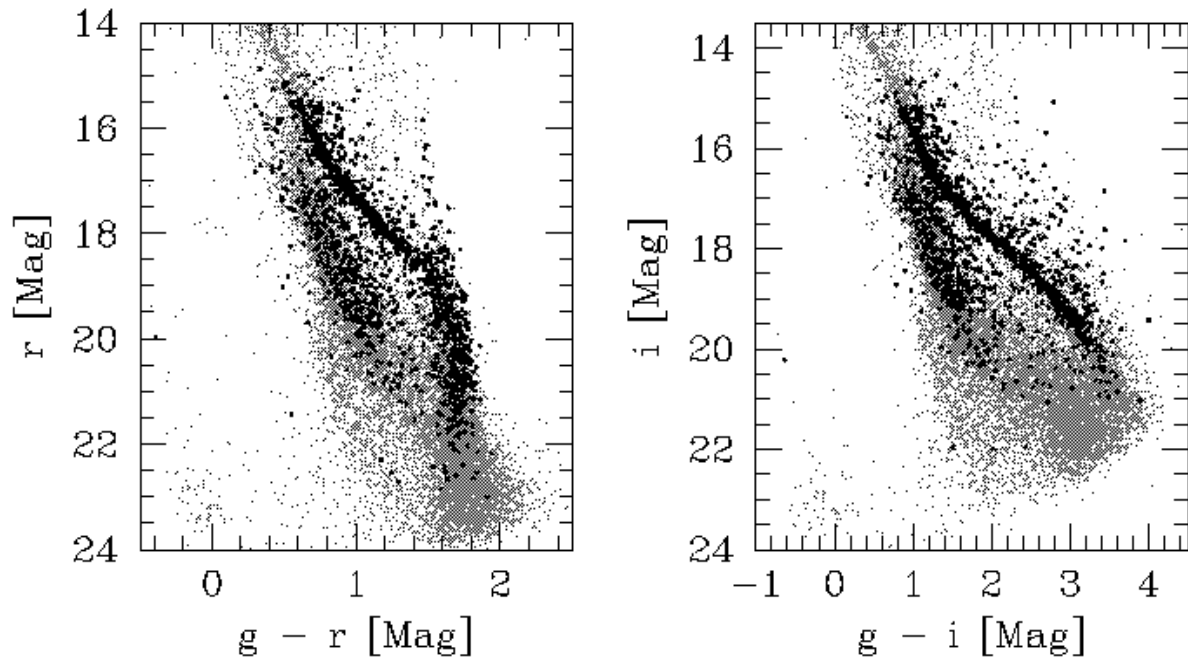


Fig. 11.— Location of identified variables on gr and gi CMDs. The dark points are the variables, the gray-scale is used to show all the point sources. The variables appear to lie preferentially along the cluster main sequence. The cut-off at the bright end is due to saturation of our primary time-series data.

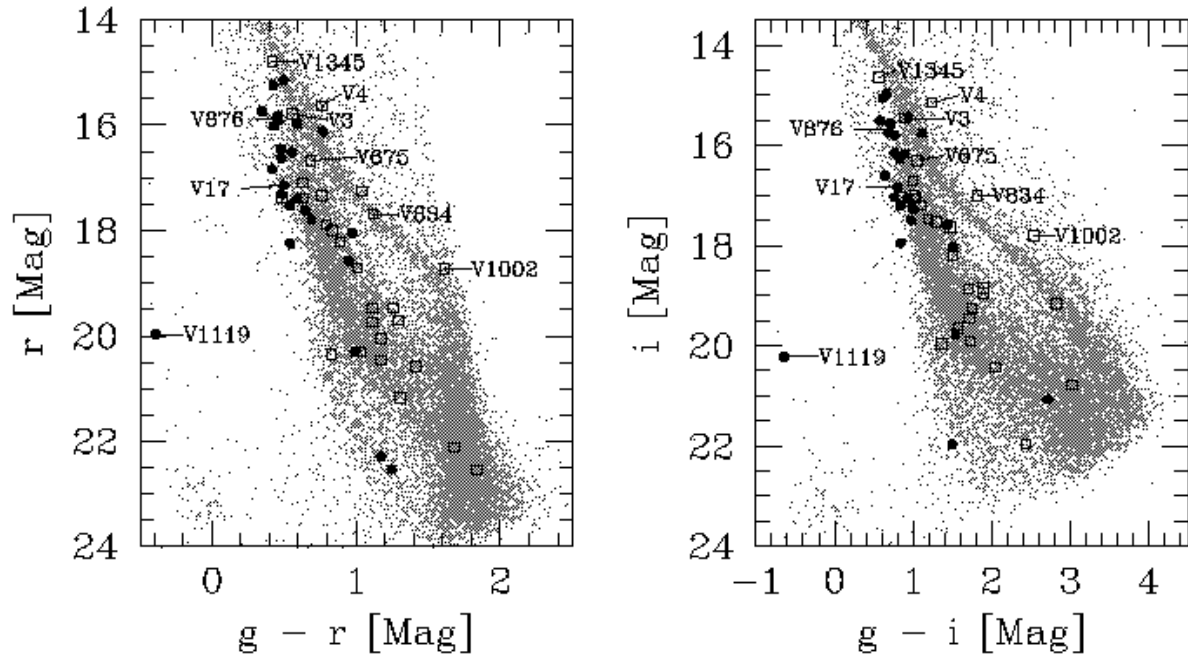


Fig. 12.— Location of visually selected short-period pulsating variables (filled points) and eclipsing binaries (open squares) on gr and gi CMDs. Labels indicate some of the variables discussed in the text. Note that we do not use a symbol to plot V876 as it is neither an eclipsing binary nor a pulsating star, the label however shows its location on the CMDs.

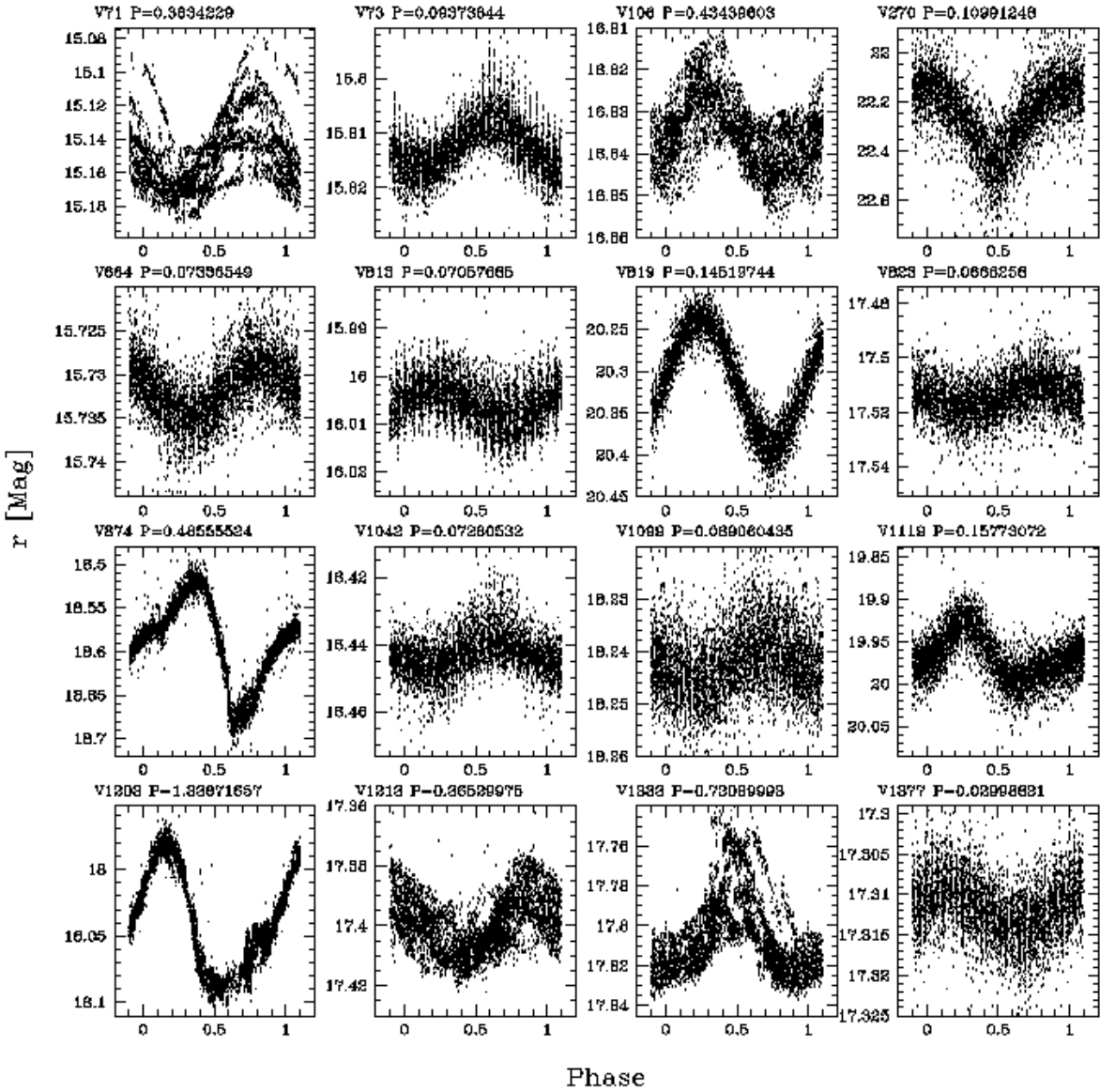


Fig. 13.— Phased light curves for 18 visually selected short-period pulsating variables.

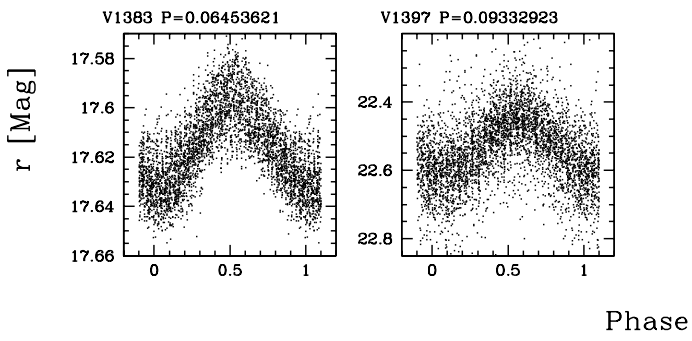


Fig. 13.— *Continued.*

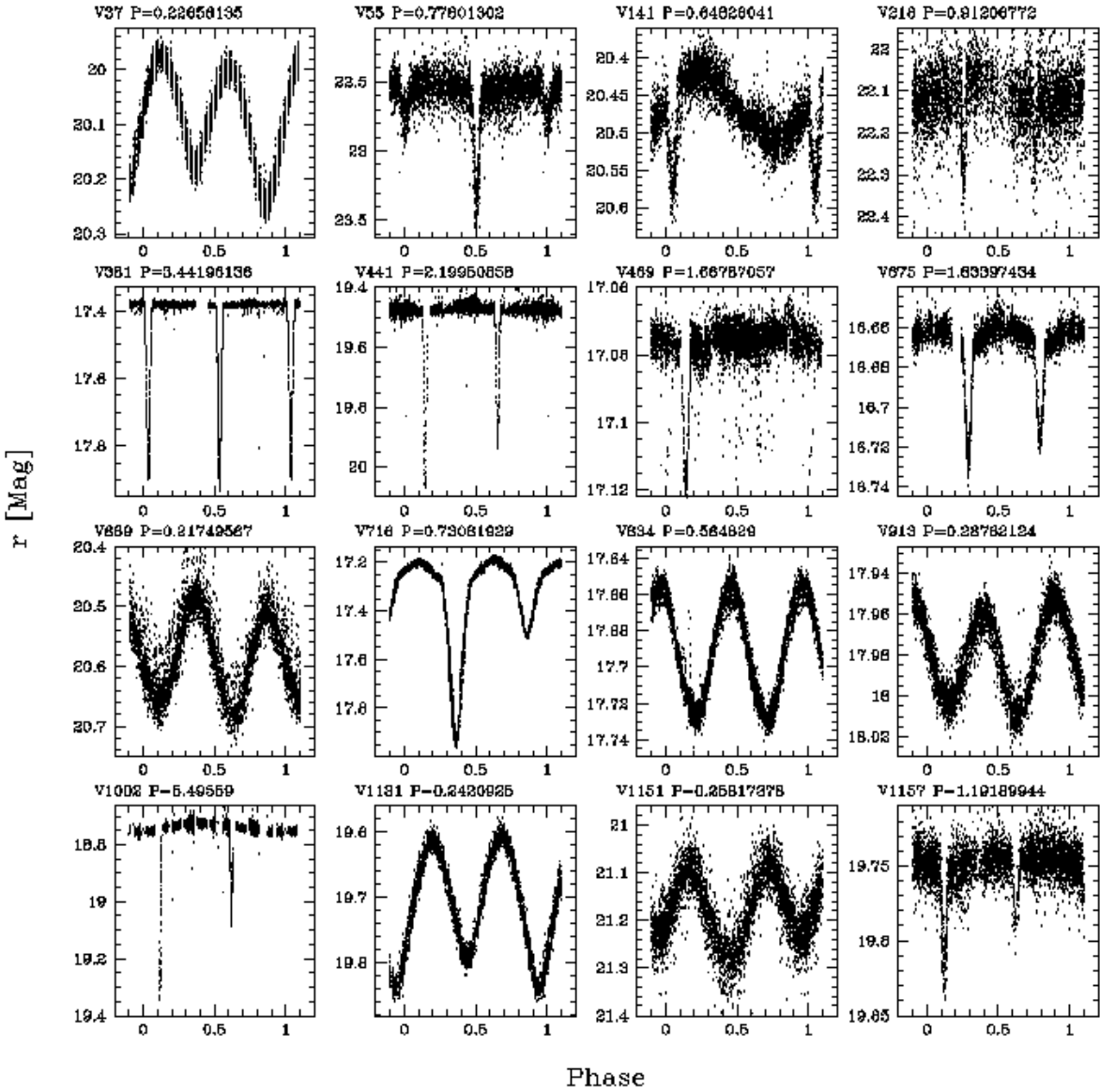


Fig. 14.— Phased light curves for 19 visually selected eclipsing binaries.

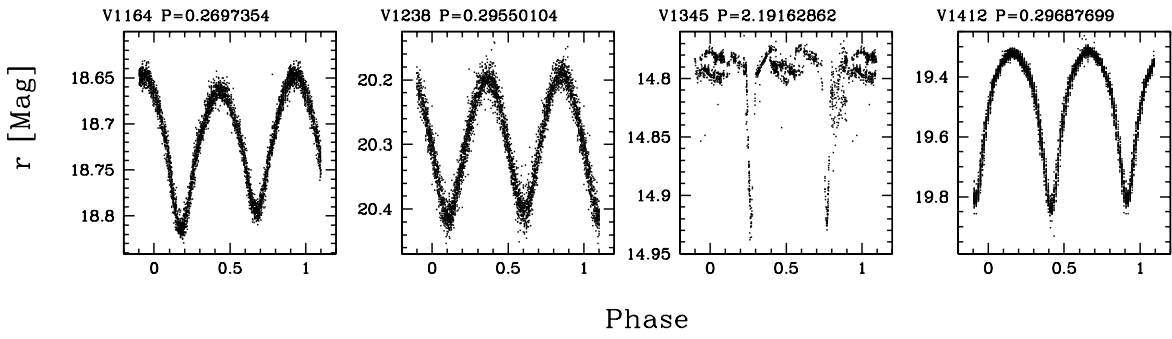


Fig. 14.— *Continued.*

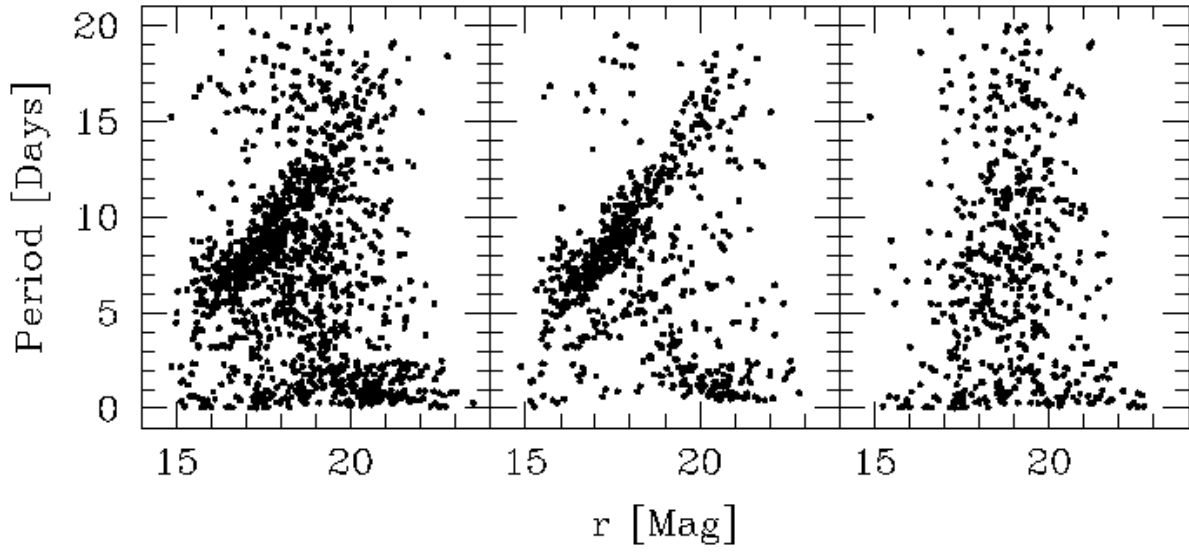


Fig. 15.— Period- r relation for (left) all variables stars, (center) photometrically selected candidate cluster members and (right) non-cluster members. Note that there is a strong correlation between period and magnitude for cluster members while for non-members there is no clear correlation.

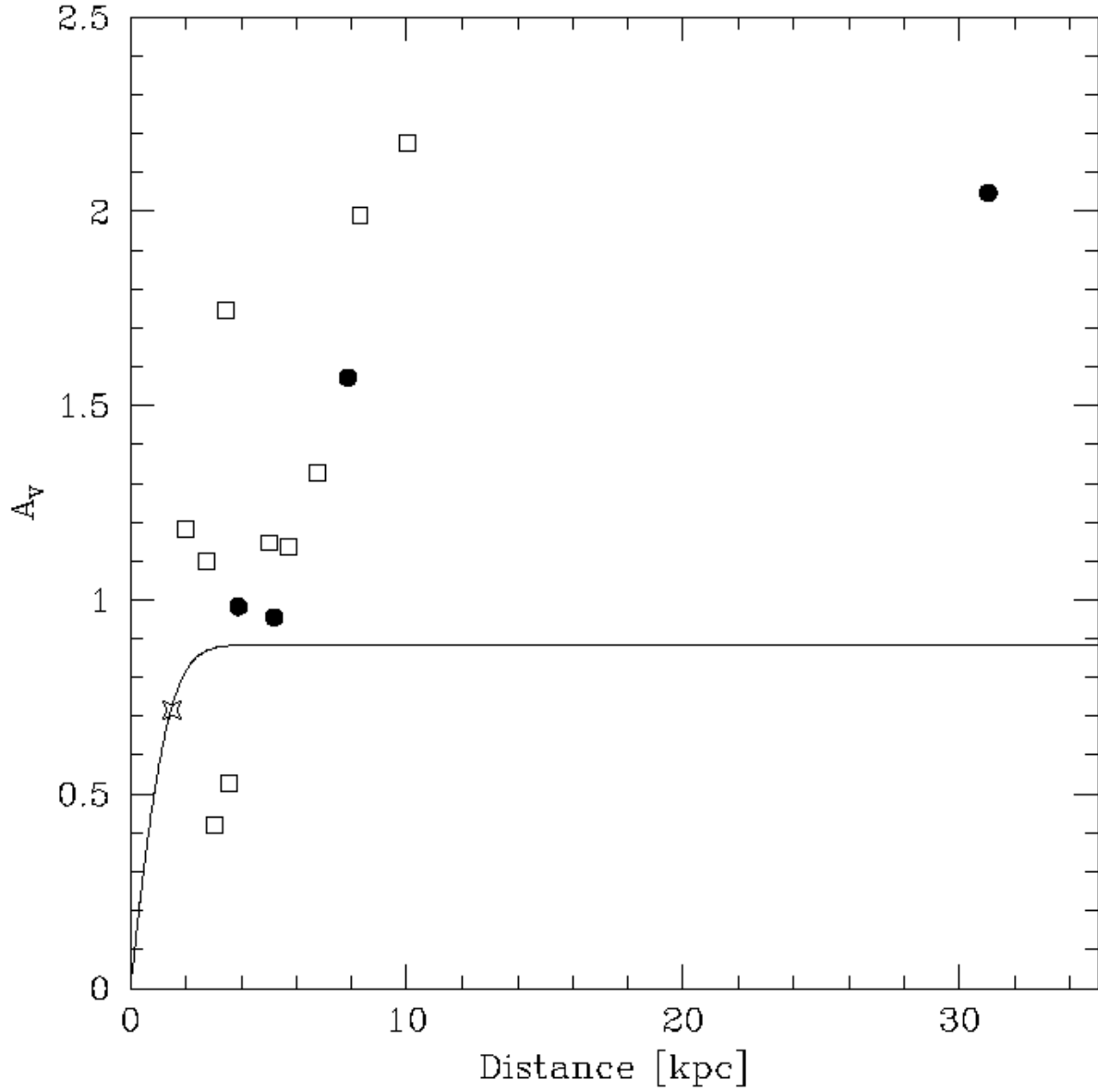


Fig. 16.— A_V vs distance for 10 W UMa eclipsing binary systems (open squares), 4 δ -Scuti stars (filled points) and the open cluster (star). The line shows the Besançon model (Robin et al. 2003) for the galactic latitude/longitude of the field, assuming an interstellar extinction of 0.7 mag/kpc.

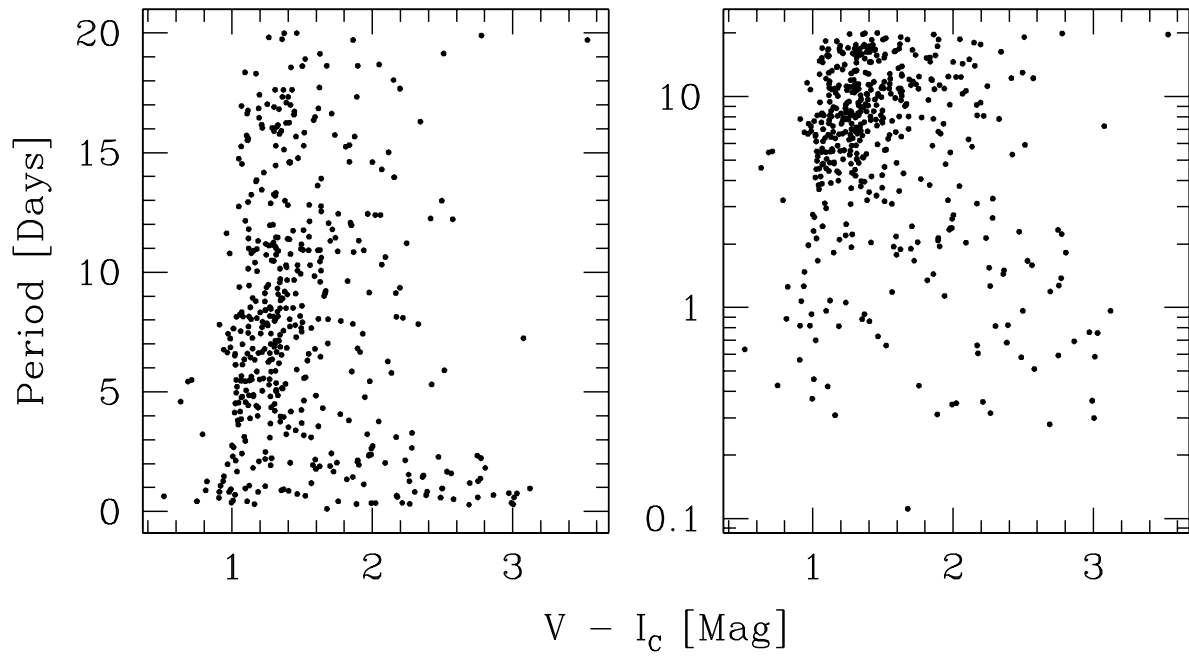


Fig. 17.— Period vs. $V - I_c$ for variable stars that are not members of the cluster, not eclipsing binaries, and not δ -Scuti or RR Lyrae type pulsators. The left panel shows the period on a linear scale, the right panel on a logarithmic scale.

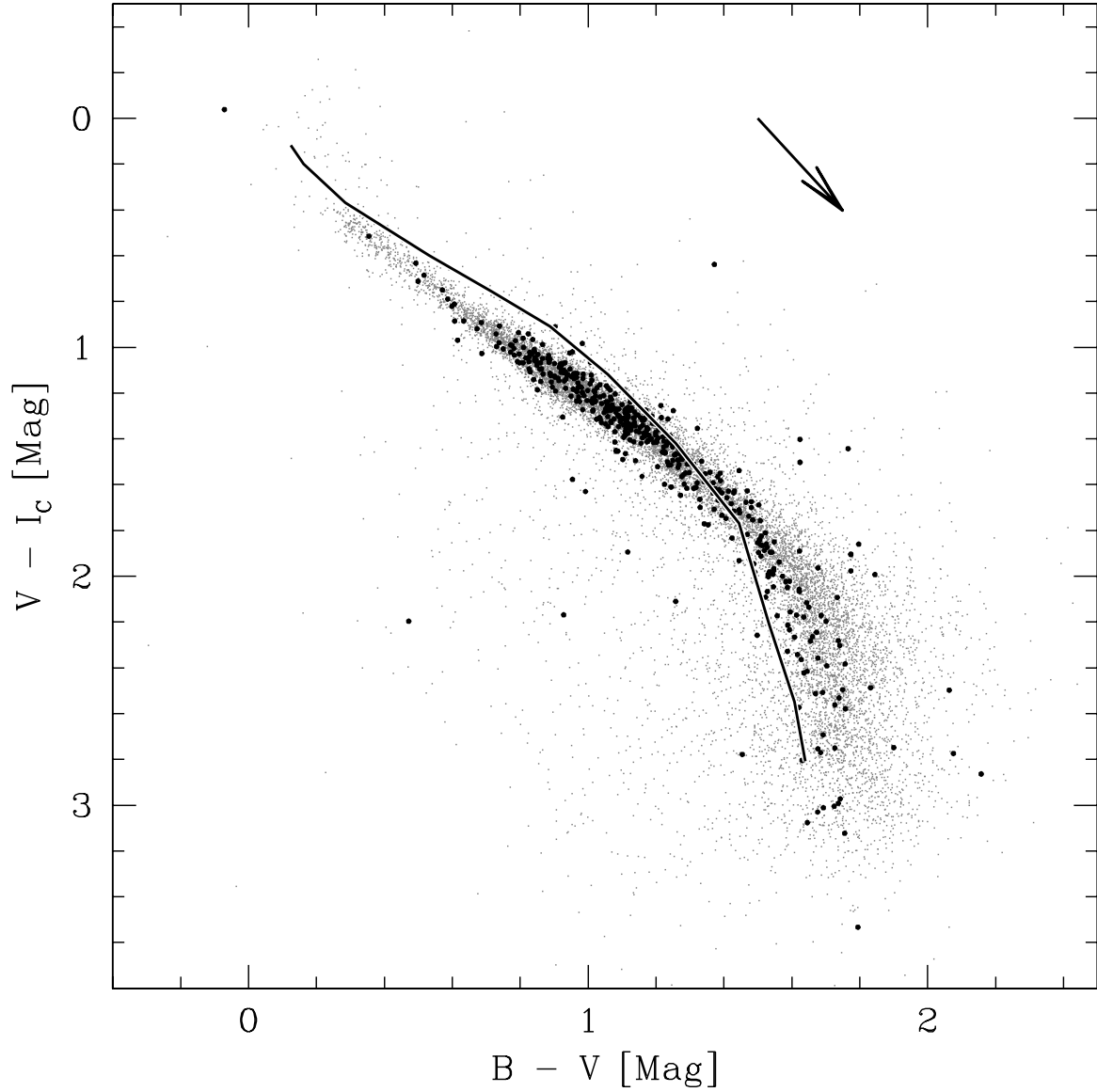


Fig. 18.— $B-V$ vs $V-I_C$ color-color plot showing all stars (gray points), field variables that are not eclipsing binaries nor obvious pulsators (dark points), and the fiducial *de-reddened* relation for the cluster (solid line). The arrow shows the direction of the reddening vector. Using this diagram we estimate the reddening to all the stars with $B-V < 1.2$, $V-I_C < 1.8$.

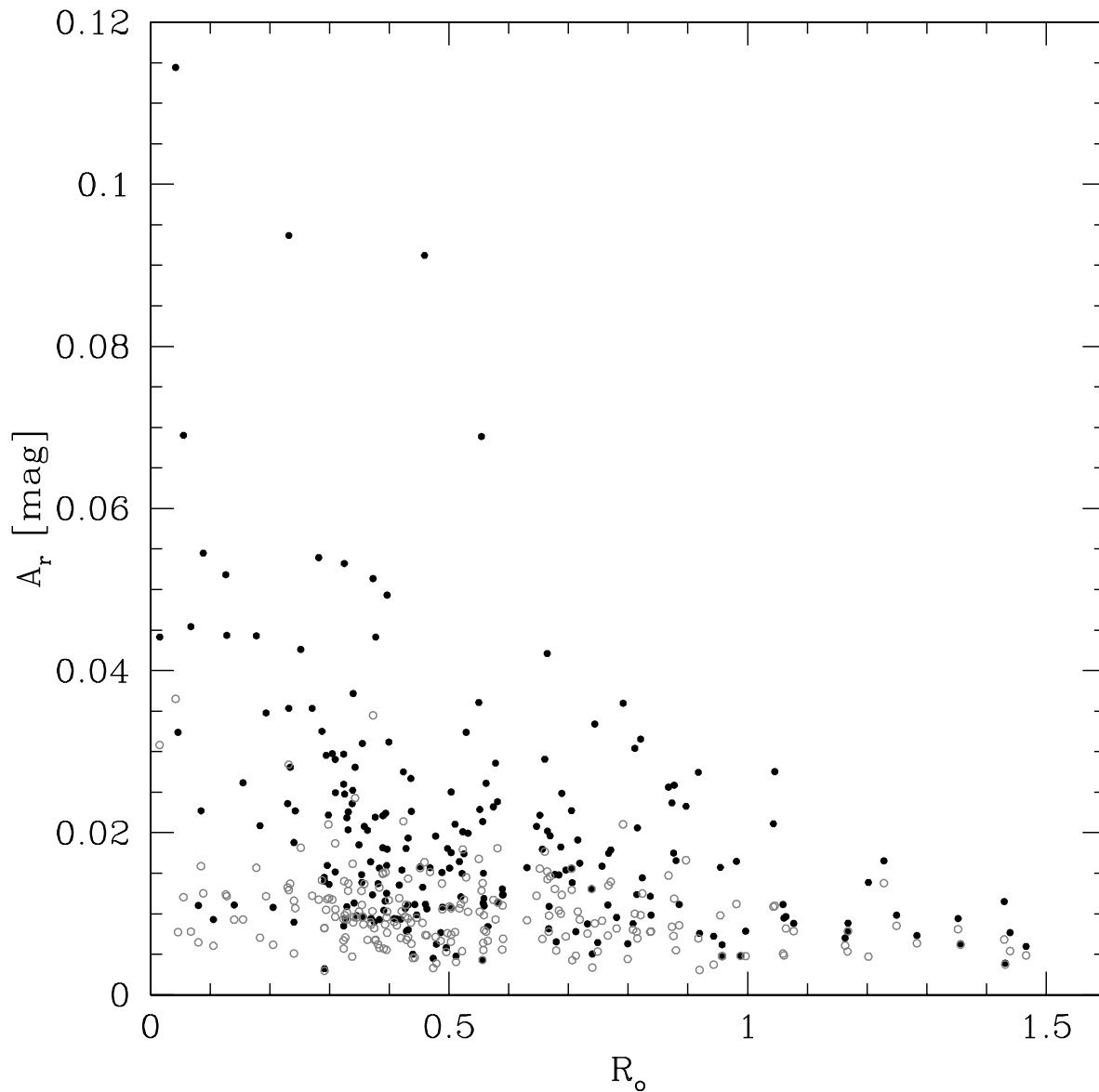


Fig. 19.— The r -band amplitude (A_r) versus the Rossby number (R_o) for field variables not classified as eclipsing binaries or pulsating stars (see text for a description of the selection). The filled points show the measured values, the open circles show the minimum amplitude that each variable could have had and still have been detected. The anti-correlation between R_o and A_r is consistent with the hypothesis that these variables are heavily spotted, rotating stars.

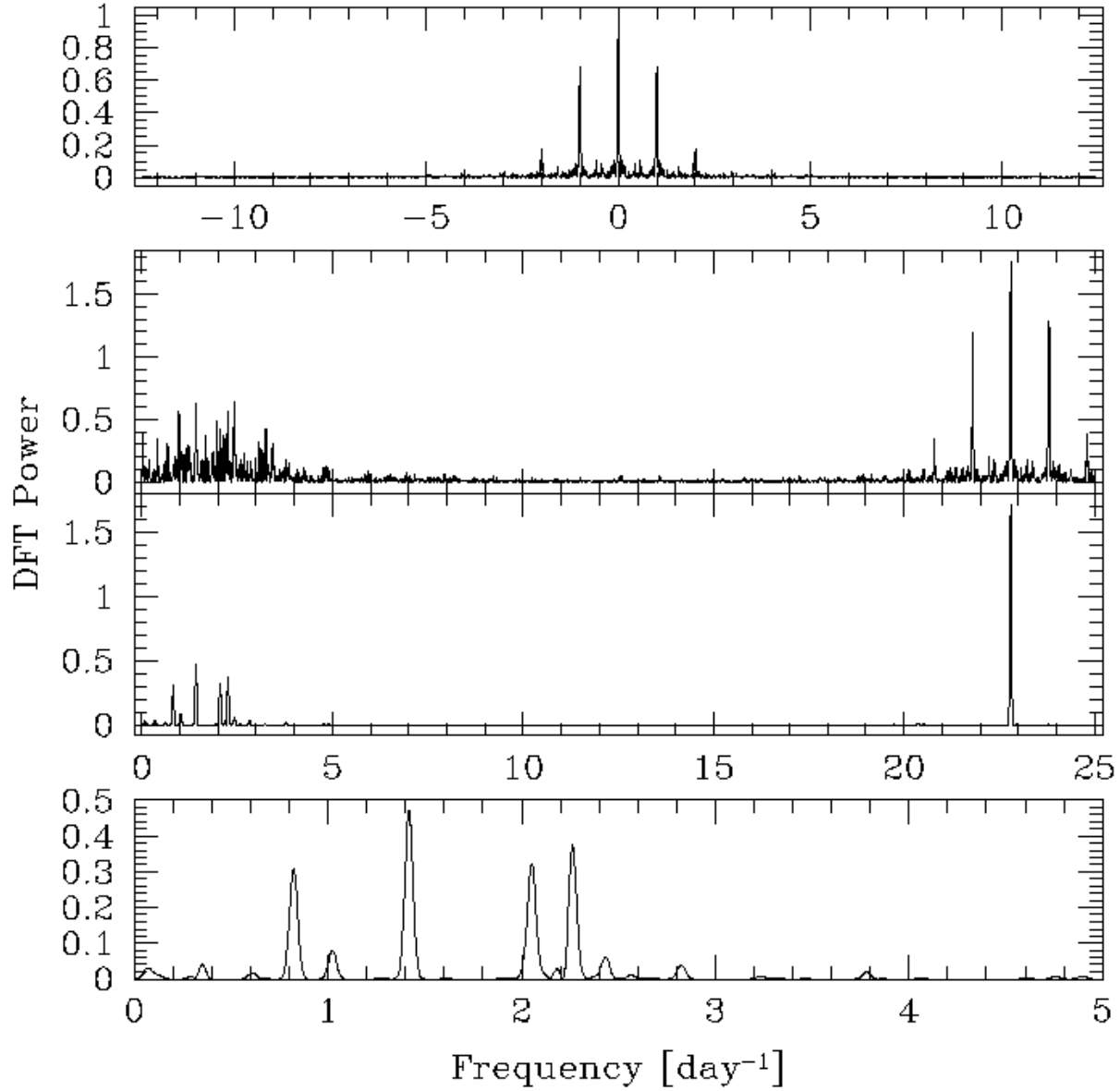


Fig. 20.— The DFT power spectrum of the light curve for V17. The top panel shows the window power spectrum, the second panel shows the raw DFT power spectrum, the third panel shows the power spectrum after implementing the CLEAN deconvolution algorithm, the bottom panel shows the CLEAN power spectrum zoomed in on the low frequency region. The bottom three plots have been scaled by a factor of 10^4 . The CLEAN power spectrum reveals five frequencies at 22.796 days^{-1} , 1.418 day^{-1} , 2.263 day^{-1} , 2.054 day^{-1} , and 0.823 day^{-1} .

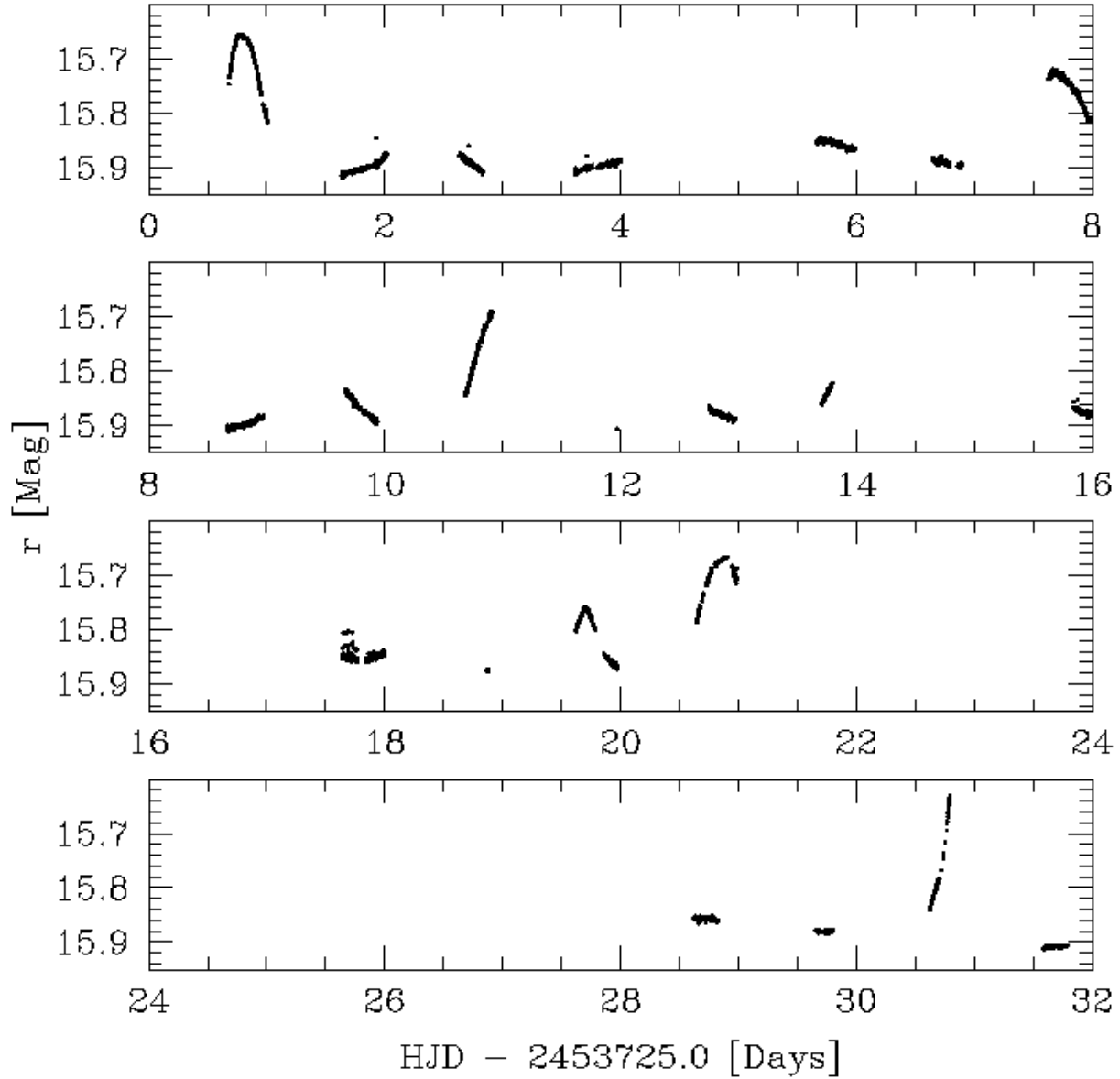


Fig. 21.— Light curve of the variable V876. The light curve is non-periodic, showing continuous variability with repeated outbursts having amplitudes of 0.1 – 0.2 mag, durations of 0.5 days and a time between outbursts of 1-2 days.

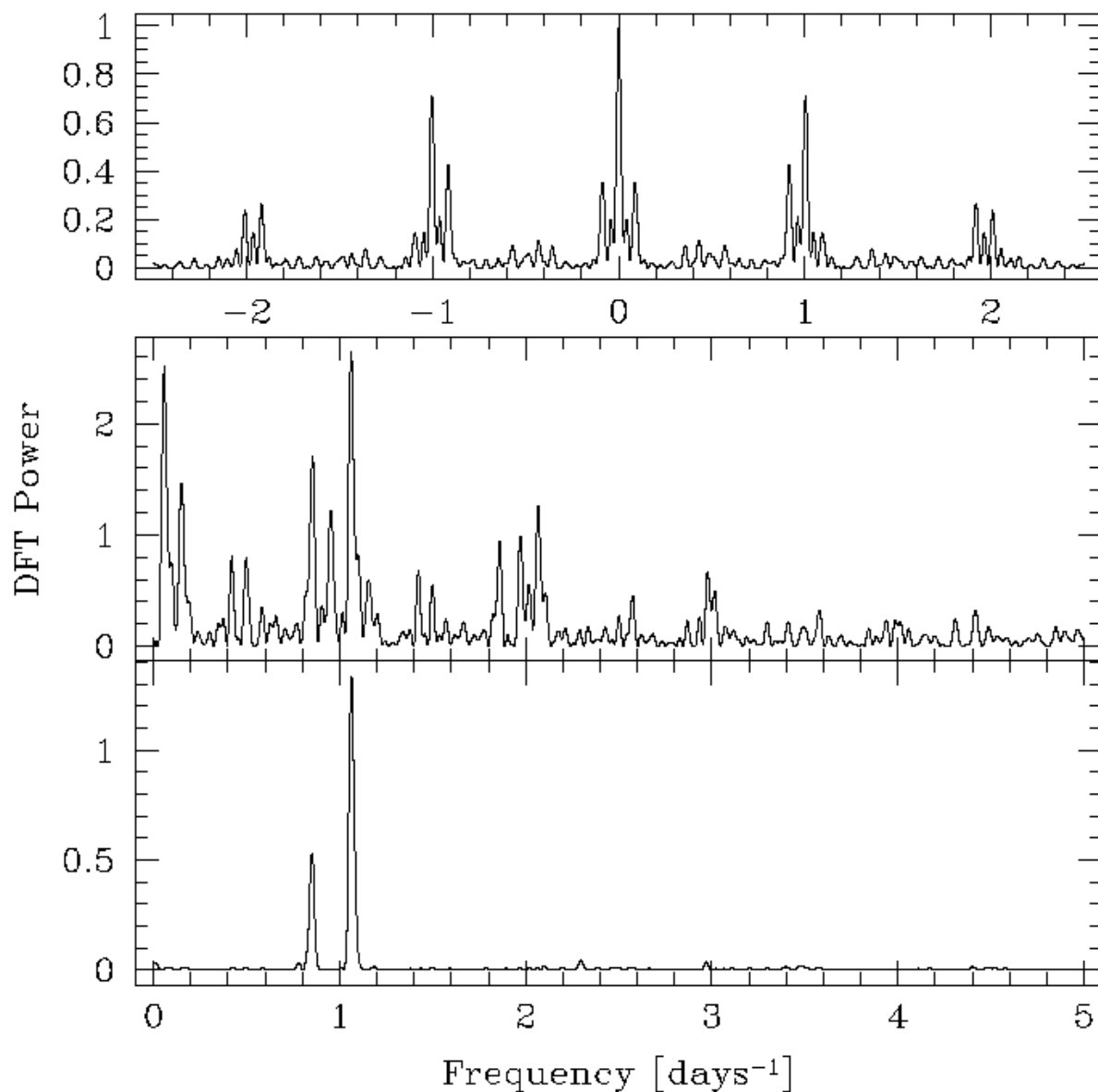


Fig. 22.— The DFT power spectrum of the light curve for the detached eclipsing binary system V1345. The top panel shows the window power spectrum, the middle panel shows the raw DFT power spectrum, the bottom panel shows the power spectrum after 10 iterations of the CLEAN deconvolution algorithm. The bottom two plots have been scaled by a factor of 10^5 . The CLEAN power spectrum reveals two strong signals, one at a frequency of $1.063 \pm 0.013 \text{ days}^{-1}$, the other at a frequency of $0.852 \pm 0.013 \text{ days}^{-1}$. These correspond to periods of $0.941 \pm 0.011 \text{ days}$, and $1.174 \pm 0.013 \text{ days}$, the same periods found by L-S.

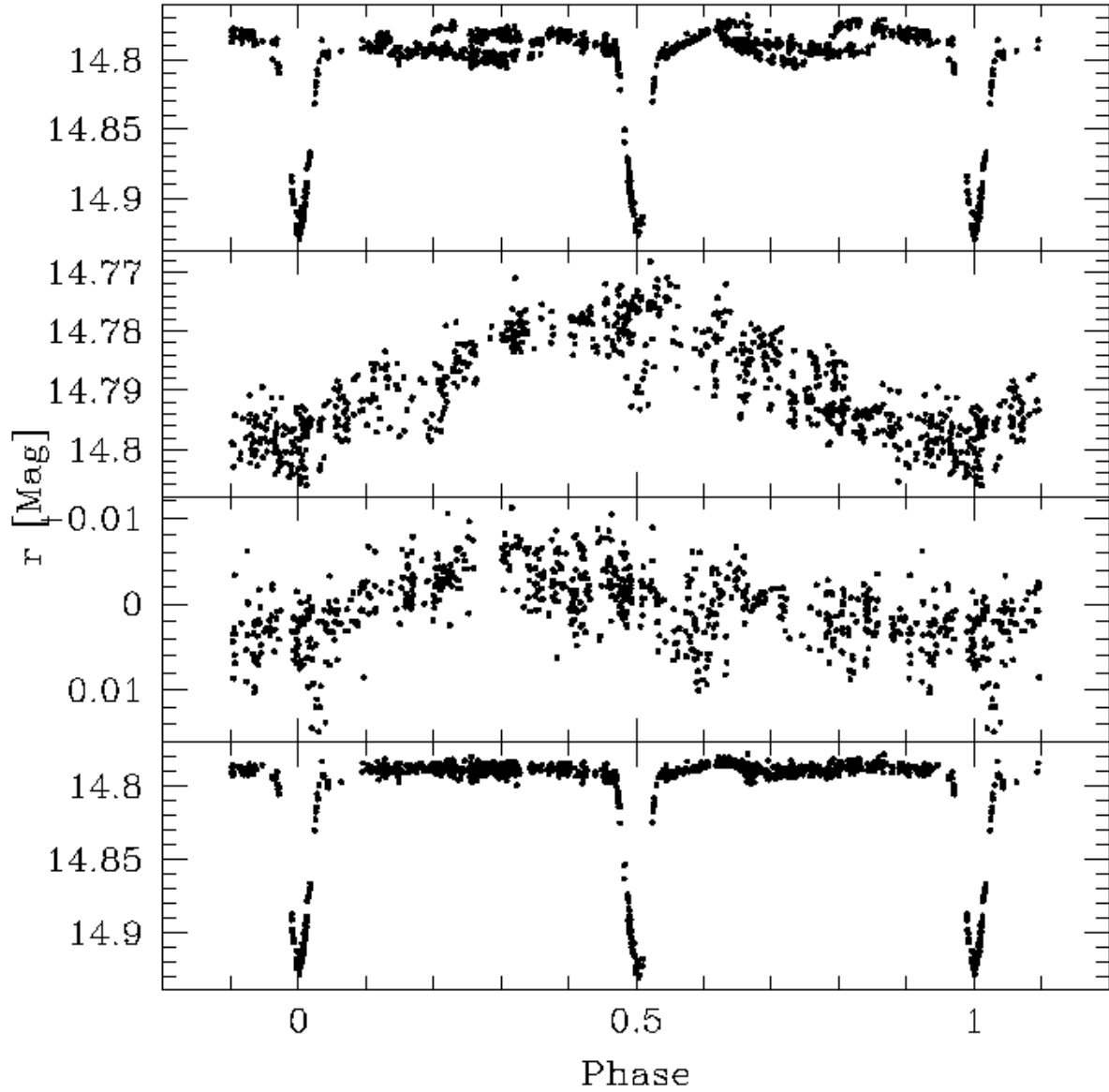


Fig. 23.— Light curve of the detached eclipsing binary system V1345. Top: phased at the orbital period of 2.1916 days. Second from top: out of eclipse points phased at 0.941 days. Second from bottom: out of eclipse points, after subtracting a sinusoid fit to the second from top plot, phased at 1.174 days. Bottom: phased at the orbital period after removing the signals in the middle two panels.

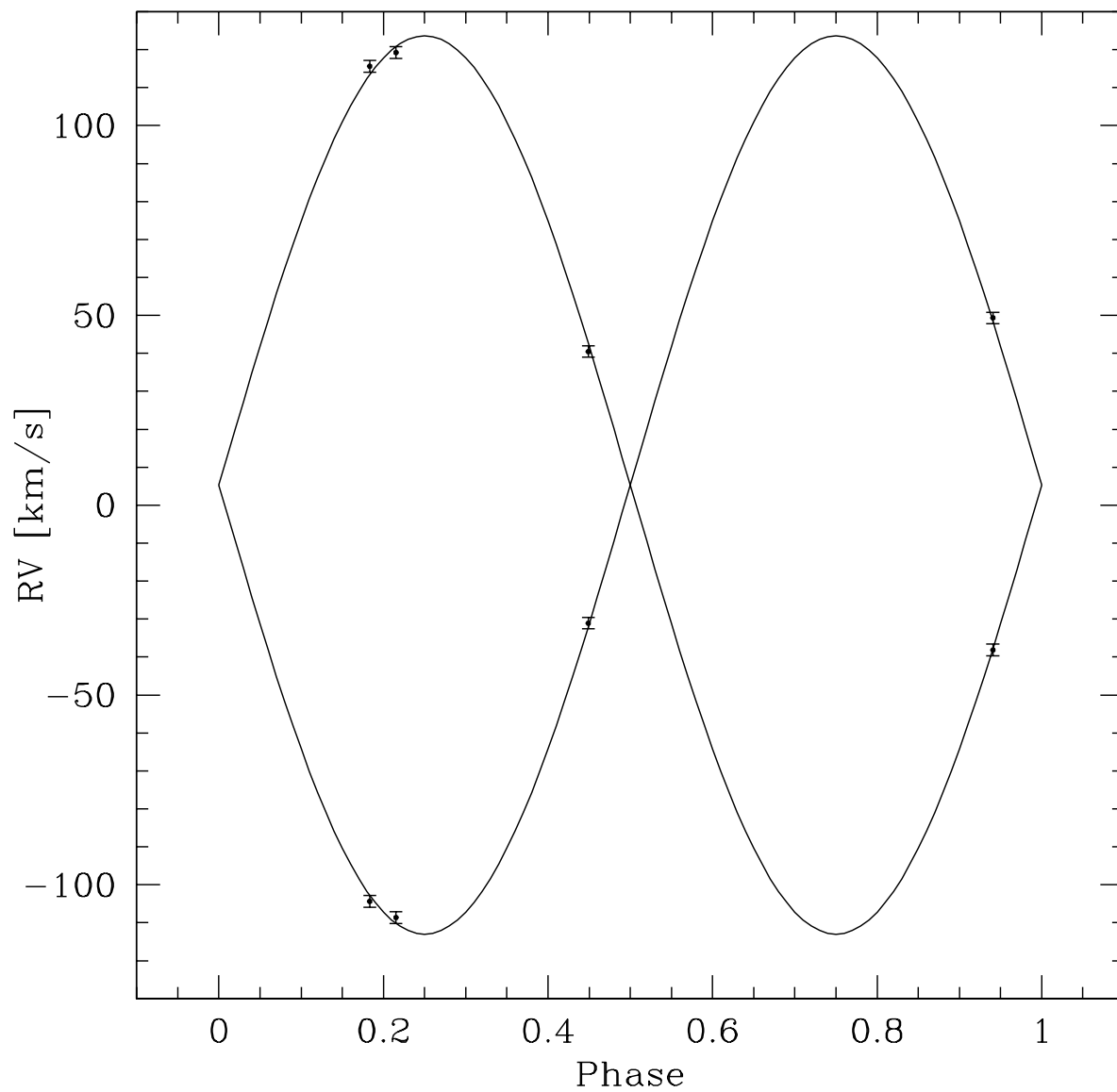


Fig. 24.— Radial velocity curves for the primary and secondary components of the double-lined eclipsing binary system V1345. The solid line shows a zero-eccentricity fit to the observations. We assume an error of 2.2 km/s for each observation. The stars have equal mass to within 1%.

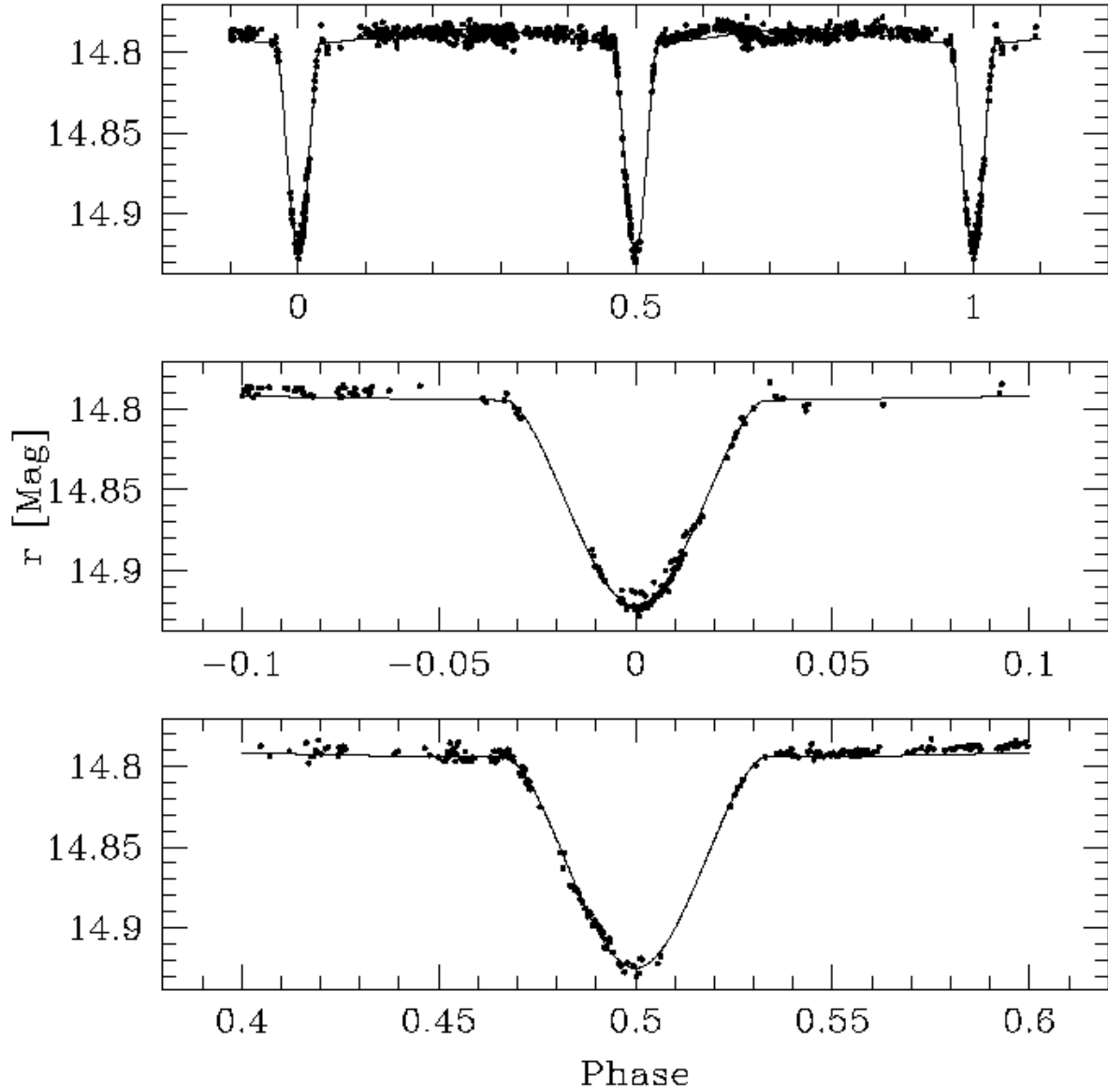


Fig. 25.— Best fit detached eclipsing binary model to the light curve of V1345. The top panel shows the full phased light curve, the bottom panels are zoomed in on the eclipses.

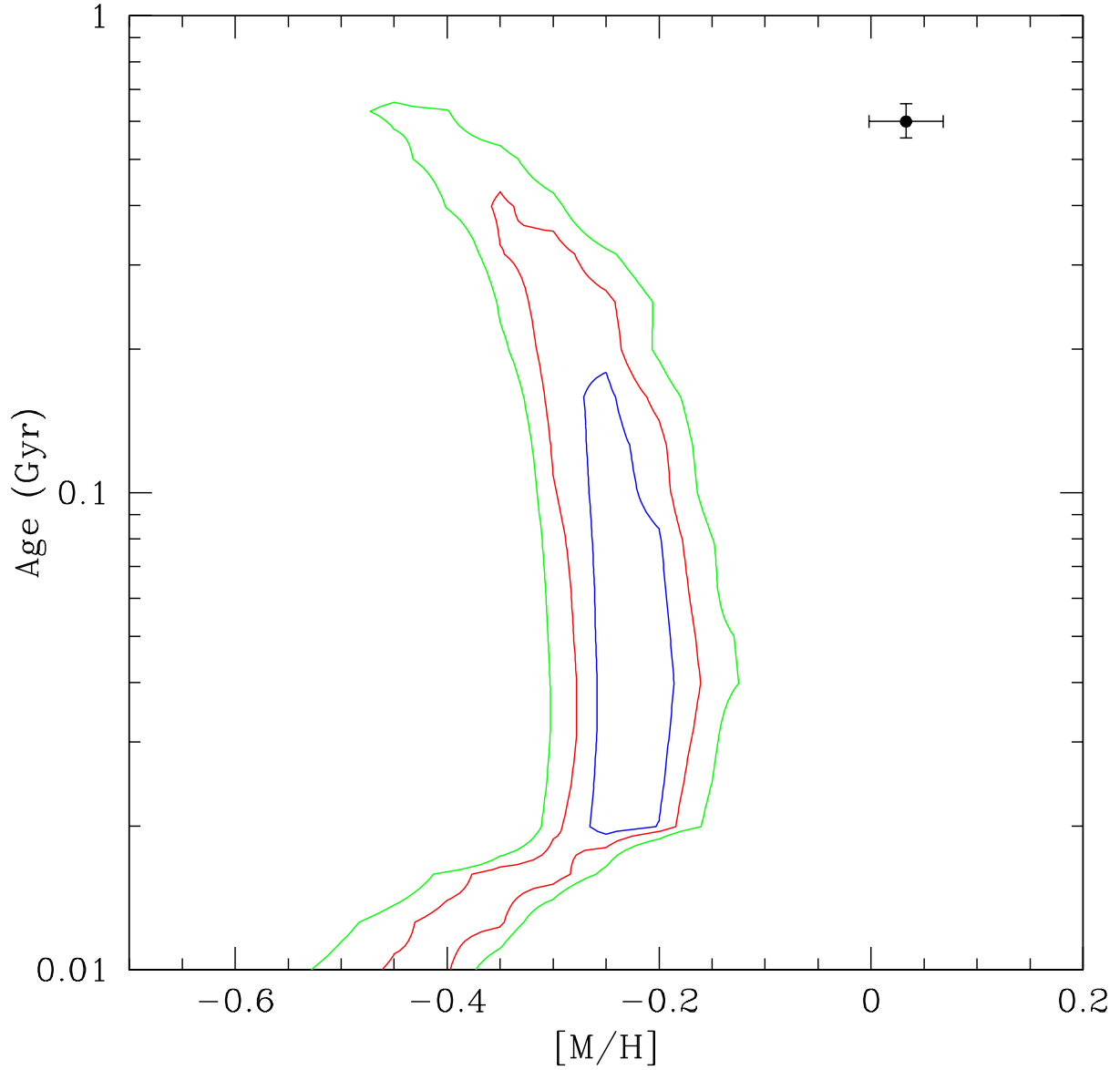


Fig. 26.— Age-metallicity contours for the eclipsing binary system V1345 from comparing the Y2 isochrones with the observed masses/radii/temperatures of the components. The contours show the 68.3%, 95.4% and 99.7% confidence levels. The point shows the values for the cluster. The binary system appears to have a lower metallicity and younger age than the cluster.

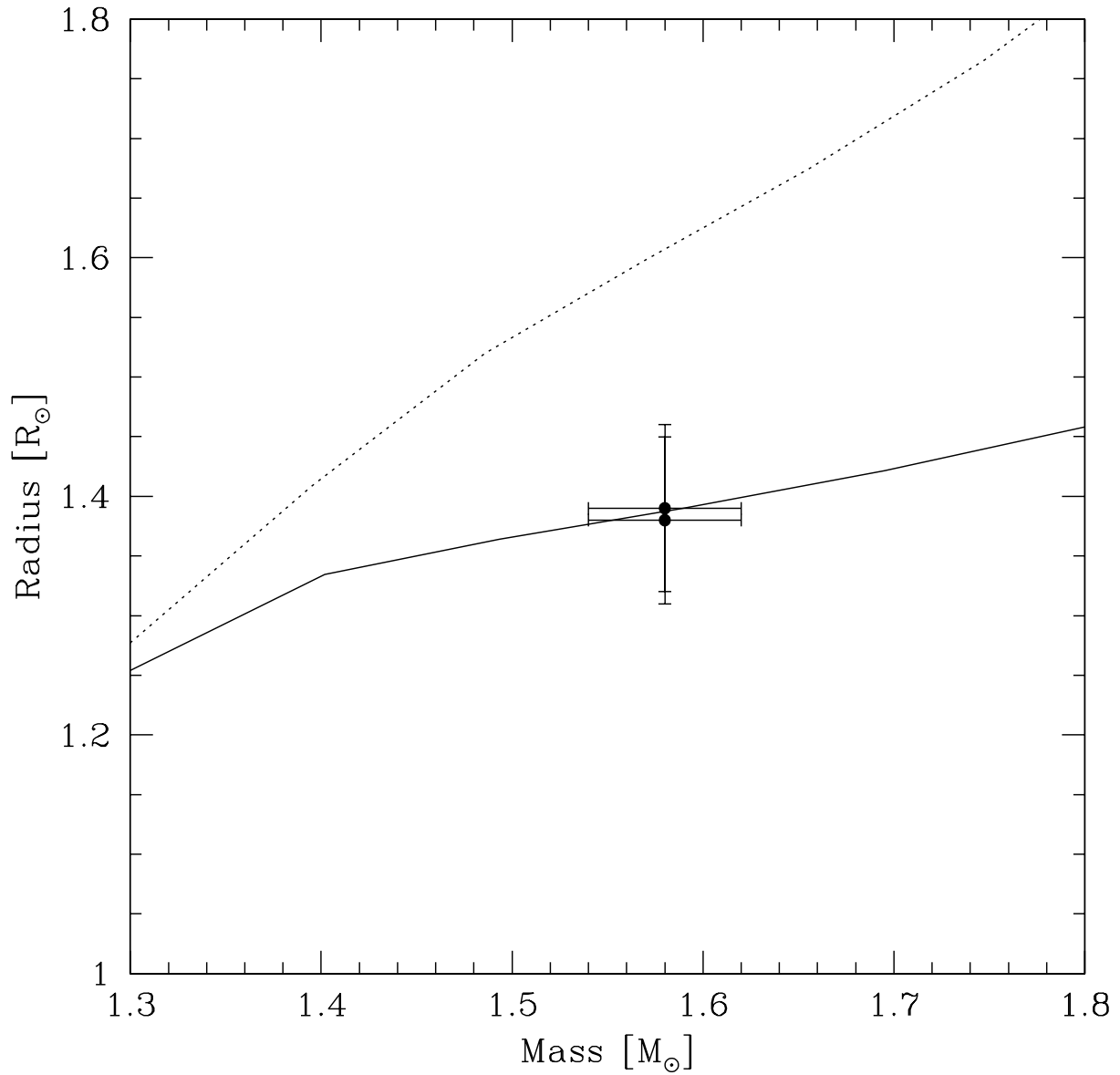


Fig. 27.— The masses and radii of the two components of V1345 together with the expected relations from the Y2 isochrones for the cluster metallicity of $[M/H] = 0.033$ and age of 600 Myr (dotted line), and for a lower metallicity of $[M/H] = -0.25$ and age of 100 Myr (solid line). The stars appear to have radii that are too small, given their masses, for them to have the metallicity and age of the cluster.

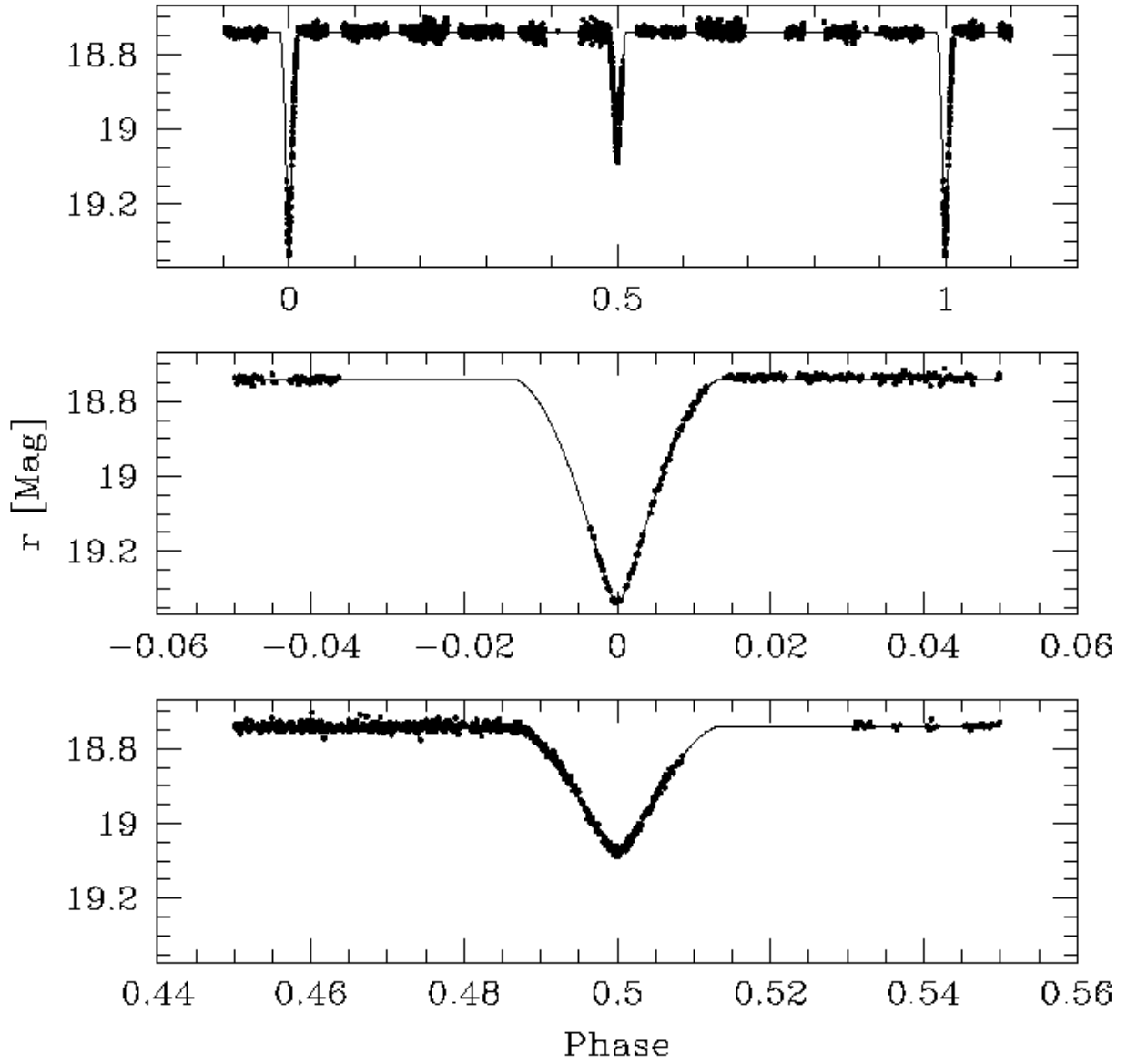


Fig. 28.— Best fit detached eclipsing binary model to the light curve of V1002. The top panel shows the full phased light curve, the bottom panels are zoomed in on the eclipses. In this plot we adopt the zero-point of phase to be the time of primary eclipse.

Table 1. Variable Star Catalog^a

ID	RA (J2000)	DEC (J2000)	Chip	Period (days)	σ_P (days)
1	05:52:20.35	+32:33:20.4
2	05:52:16.54	+32:28:15.7
3	05:52:33.01	+32:32:42.0	14	0.42248314	0.00001000
4	05:52:53.26	+32:33:01.5	5	0.55819369	0.00002600
5	05:53:00.64	+32:24:50.8	8	0.27878242	0.00000400
6	05:51:50.53	+32:32:34.8	23	0.10983967	0.00000100
7	05:52:39.09	+32:36:31.2	13	0.35773482	0.00000400
8	05:52:34.32	+32:32:18.7	...	0.11950000	...
9	05:52:14.91	+32:24:41.0	...	0.09085950	...
10	05:52:00.49	+32:36:48.2	...	0.07843140	...

^aThe complete version of this table is in the electronic edition of the Journal. The printed edition contains only a sample.

Table 1. Continued

$\langle r \rangle$ (mag) ^a	RMS_r (mag) ^b	g (mag)	r (mag) ^c	i (mag)	B (mag)	V (mag)	Type ^d	Selection ^e
...	14.015	13.406	10	000
...	15.341	14.653	10	000
15.7511	0.1057	16.350	15.789	15.460	16.779	16.051	10	111
15.6407	0.0815	16.396	15.634	15.157	16.886	15.948	10	111
15.9035	0.1140	16.374	15.915	15.433	16.769	16.184	01	111
15.9552	0.1263	16.564	15.973	15.800	01	111
17.3113	0.1562	18.290	17.252	17.195	18.705	17.890	10	111
...	12.925	12.498	01	000
...	13.668	13.298	01	000
...	15.293	14.762	01	000

^aThe flux averaged r magnitude of the light curve.

^bThe root-mean-square of the light curve.

^cThe r magnitude of the source in the photometric catalog (Paper I)

^dA two-bit flag. The first bit denotes whether or not the star is an eclipsing binary. The second denotes whether or not it shows pulsations.

^eA three-bit flag. The first bit denotes if the variable was selected by LS, the second if it was selected by AoV and the third if it was selected by BLS.

Table 2. Summary of Variable Star Catalog

	Number
Total	1419
Previously Known	24
Total Detected in Survey	1409
Recovered Previously Known	14
New Discoveries	1395
Eclipsing Binaries	28
Pulsating Variables	27
With <i>BVgri</i> Photometry	1344
Near <i>gri</i> main sequence	738
Near <i>BVgri</i> main sequence	518

Table 3. Extinction and Distances for Fundamental Mode δ -Scuti Stars

ID	V	$B - V$	$V - I_C$	Period (days)	A_V	Distance (kpc)
V5	16.184	0.585	1.194	0.2787824	1.57	7.87
V6	16.177	0.691	0.806	0.10984	0.95	5.20
V11	15.456	0.452	0.826	0.1186712	0.98	3.90
V819	20.695	1.711	1.377	0.1451974	2.05	31.02

Table 4. Extinction and Distances for W UMa Eclipsing Binaries

ID	V	$B - V$	$V - I_C$	Period (days)	A_V	Distance (kpc)
V3	16.051	0.728	1.026	0.4224831	1.10	2.74
V4	15.948	0.938	1.234	0.5581937	1.18	2.01
V7	17.890	0.815	1.117	0.3577348	1.15	5.02
V20	17.628	0.892	1.008	0.2894559	0.42	3.05
V24	20.506	1.275	1.518	0.2526742	1.14	5.75
V834	18.156	1.227	1.617	0.5648290	1.74	3.49
V1131	20.234	1.134	1.435	0.2420925	1.33	6.77
V1151	21.847	1.402	1.871	0.2581738	2.18	10.05
V1164	19.030	1.136	1.267	0.2697354	0.53	3.56
V1412	19.930	1.066	1.535	0.2968770	1.99	8.31

Table 5. Radial velocity and light ratio measurements from the spectra of V1345.

HJD	Primary Velocity [km/s]	Secondary Velocity [km/s]	Light Ratio [L_2/L_1]
2454154.6776	-104.36	115.64	0.991
2454165.7104	-108.62	119.24	0.955
2454170.6082	-31.08	40.47	0.995
2454171.6861	49.34	-38.14	1.025

Table 6. Eclipse time measurements for V1345. The last measurement given is inferred from a fit to the radial velocity data.

Eclipse Number	Observed Minimum [HJD]	Error [HJD]
0.5	2453725.6289	0.0008
1.0	2453726.7223	0.0004
1.5	2453727.8188	0.0003
2.0	2453728.9160	0.0004
7.5	2453740.9756	0.0003
195	2454152.0803	0.0037

Table 7. Parameters for Eclipsing Binary V1345.

Parameter	Value	Error
P_{orb}	2.19258 days	0.00004 days
HJD_0	2453724.5306	0.0004
K_1	118.3 km/s	1.3 km/s
K_2	118.3 km/s	1.3 km/s
γ	5.3 km/s	0.7 km/s
J_S/J_P	1.02	0.02
$(R_P + R_S)/a$	0.266	0.002
R_S/R_P	0.99	0.1
i	80.00°	0.09°
a	10.41 R_\odot	0.23 R_\odot
M_1	1.58 M_\odot	0.04 M_\odot
M_2	1.58 M_\odot	0.04 M_\odot
R_1	1.39 R_\odot	0.07 R_\odot
R_2	1.38 R_\odot	0.07 R_\odot

Table 8. Light Curve Parameters for V1002.

Parameter	Value	Error
$P_{orb} = P_{rot}$	5.49378 days	0.00005 days
HJD_0	2453725.6989	0.0001
J_S/J_P	0.649	0.004
$(R_P + R_S)/a$	0.0855	0.0003
R_S/R_P	0.95	0.01
i	89.73°	0.05°
L_3	0.266	0.006